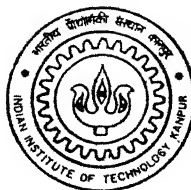# A Preliminary Investigation on the Correlation of Microstructural Parameters with Texture in Ni-10%Co Alloy

by
Yojna Purohit
(9810625)

DEPARTMENT OF MATERIALS AND METALLURGICAL ENGINEERING
INDIAN INSTITUTE OF TECHNOLOGY KANPUR
May, 2000

A Preliminary Investigation on the Correlation of Microstructural Parameters with Texture in Ni-10%Co Alloy

A thesis submitted

in Partial Fullfilment of the Requirements

for the Degree of

MASTER OF TECHNOLOGY

by

Yojna Purohit

(9810625)

to the

Department of Materials and Metallurgical Engineering

INDIAN INSTITUTE OF TECHNOLOGY, KANPUR

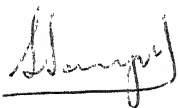**May, 2000**

CERTIFICATE

This is to certify that the present work , entitled **A Preliminary Investigation on the Correlation of Microstructural Parameters with Texture in Ni-10%Co Alloy** *by* Ms. Yojna purohit (9810625) has been carried out under my supervision and to the best of my knowledge it has not been submitted elsewhere for a degree.

Dr.S. Sangal
Dept.of Materials & Metallurgical Engg.
Indian Institute of Technology
Kanpur

Date: May 2, 2000

Acknowledgement

It is a great pleasure to express my sense of gratitude and indebtness to my thesis supervisor Dr.S.Sangal for his able guidance, valuable suggestions and constant encouragement during different phases of the investigation and preparation of this thesis.

I would also very much like to express my greatfulness to Prof. R.K.Ray for his suggestions and guidance in analysing the texture part of the work. I am thankful to him for allowing me to sit and use his laboratory facility.

I acknowledge Mr.Kumar and Mr.K.P.Mukherjee for their various help at different stages of the experimental work.

I express my heartiest greatfulness to Swami Adhyatma Chaitanya for invigorating me with his strengthening words. I am also extremely thankful to Dr.S.Sangal and his wife Mrs. Rita Sangal for their help and support during my hard days.

I acknowledge the most important contribution of my family and friend Nishith Rohatgi for their continuous encouragement and cooperation. Without their names my thesis is incomplete.

My sincere thanks are due to my friends Aruna, Mansiz, and especially Rohitaswa Prasad and Chandrashekhar, for helping me in the preparation of my thesis. Finally, I thank Rashmi Ray who gave me a wonderful association and a truly friendly atmosphere.

May, 2000   Yojna Purohit

IIT kanpur   (9810625)

Contents

References

Abstract

Since, the same manufacturing processes give rise to the microstructural and texture characteristics of a material, a correlation between the nature and sharpness of the crystallographic texture of the material and its microstructure is generally expected. But there has hardly been any attempt so far to bring out this correlation. In this work a preliminary investigation on the correlation of Microstructural parameters with Texture in Ni-10%Co alloy has been done. For this purpose of correlating the two, spatial grain size distribution, dihedral angles and grain boundary energy distribution and fractal dimensions of the 95%cold rolled Ni-10%Co alloy have been determined and than attempts were made to correlate them with texture data of the alloy.

Spatial grain size distribution has been determined from linear Intercept distributions using a Matrix method based on a tetrakaidecahedron grain model. The mean, standard deviation and 95% confidence interval of the intercept length distribution were analysed which suggested that the increase in the grain size is ststistically significant. Plots of normalised cumulative frequency of intercepts length distribution of different annealed samples implies, that except for 50 hours annealed sample, the grain size distribution is similar in all the samples and the differences in the dimensions of the microstructures are related to each other by a scale factor.The intercept lenght distribution was transformed to Spatial (3D) distribution of grain diameter. The transformed distributions showed a lot of scatter and hence no comparisons were possible. This is attributed to the fact that in the case of transformed distributions, some of the values of relative frequencies were negative, which might have occurred due to errors in intercept length measurement , as they were measured manually from micrographs. The negative relative frequencies were converted to zero and the distribution was normalised.

As the relative grain boundary energy distribution in polycrystals is an important microstructural paramete a new method was used in order in order to analyse

relative energies of grain boundaries. In the 3D structure of polycrystals, the three grain boundary surfaces meet along a line (termed as a triple edge). In general the energies/area of these three surfaces will be γ_1 γ_2 and γ_3 The distributions of energy ratios γ_3/γ_1 and γ_2/γ_1 were determined by estimating the distribution of angles between grain boundary surfaces at a triple edge. It was found that the distributions tend towards 1 with annealing time and this suggested that the equilibration of random grain boundaries occur during annealing. Thus all grain boundaries would have similar energies. When the texture data was examined it was found that the volume fraction of dominating cube {100}<001> component is almost same and doesn't vary much with annealing. Thus, as all the boundaries have similar energies, it is clear that none of the grains have an advantage of preferential growth, thus keeping the volume fraction of the cube component more or less same.

Variation of fractal dimension, D, was analysed as a function of annealing. For rugged profiles the value of fractal dimension D lie between 1 and 2 . As for each of the sample the fractal dimension is close to 1, which suggests that the grain boundaries are not rugged.

Thus, an important conclusion of the work is that a correlation between texture and grain boundary energy distribution is possible. In this investigation this conclusion is further strengthened by the fact that the grain size distribution and fractal dimensions have been found to be similar in all the samples and the only parameter that varied with annealing is the relative grain boundary energy ratios.

Chapter 1

Introduction and Objectives

Stereological and Textural measurements have been used with varying degree of successes in predicting the mechanical properties of polycrystals. Since it is the same manufacturing process which give rise to the texture and microstructural characteristics of a material, a correlation between the two have been expected. Although, much study has been done seperately, on the microstructural as well as textural changes during the manufacturing process, not many attempts have been made to correlate the two.

With this objective of (correlating the two) an investigation involving quantitative microscopic characterization, of the 95%cold rolled Ni-10%Co alloy has been undertaken in the present work and attempts were than made to correlate the microstructures and the crystallographic texture of the alloy.

It is well recognized that grain boundary structure and energy plays an important role in the properties of single phase polycrystals. Reasonable mechanical properties can be achieved by controlling the grain boundary structure and grain size. The grain boundary energy state influence the strengthening properties of polycrystals significantly. Grain boundary curvature and true dihedral angles i.e., angle between grain boundary planes meeting at a triple edge in three-dimensional structure of polycrystals) are both indicators of the energy state of the grain boundaries. True dihedral angle distribution as a microstructural parameter has not generally been used because of the experimental difficulty in its measurement. However a recently developed technique [16] makes it possible for the measurement of true dihedral angles rather simply. From the true dihedral angle distribution relative energies of grain boundaries can be determined. Grain boundary energy ratios can be easily determined and this could be significantly used to predict the Texture of the material.

A very important parameter, which has been mostly neglected ,is the ruggedness of the grain boundaries. Non-availability of a suitable microstructural parameter to measure the ruggedness of these grain boundaries may be reason for this neglect. The concept of Fractal geometry serves as an efficient tool to characterize the rugged boundaries

The objectives of the present work are:

1. Characterization and evolution of microstructures as a result of thermal treatment of single phase polycrystals. For this purpose, determination of spatial grain size distribution, Dihedral angles and Relative grain boundary energy distributions and Fractal dimensions have been proposed.

2. To analyse relative grain boundary energy distributions

3. To correlate Microstructural parameters with Texture .

In order to achieve the above objectives, 95% cold rolled Ni-10%Co alloy has been chosen as a model single phase polycrystalline material.

Chapter 2

Literature Review

2.1 Techniques of quantitative microstructural characterization.

2.1.1 Matrix method for the determination of spatial grain size distribution.

Methods for determining the three-dimensional grain size distributions from planar sections employ either area distributions [1,2] or intercept distributions [3,4]. The former are more tedious. Most of these methods ignore the actual grain shapes and assume them to be spherical or ellipsoidal, e.g.cahn and fullman's method based on sphere chord distribution data was employed to determine the grain size distributions in Mgo and Al_2o_3. As the spherical grain model is unrealistic [5,6] successive subtraction techniques based on sectional area distributions and, later, on intercept distributions in a tetrakaidecahedron grain model were developed. However, successive subtraction techniques suffer from the drawback of accumulating errors. The calculations should start with the largest intercept groups. These are usually the few grains in which the relative error is large. Hence a matrix approach was developed.

Intercept length distribution for a tetrakaidecahedral grain previously shown by Haroun [5] is given in Table 2.1. A distribution : N_1, N_2, N_3, ...N_8 of three dimensional grains of sizes D_1, D_2, D_3.........D_8. was assumed. On sectioning , the largest size grains D_1 will contribute $0.365N_1$ intercepts of size l_1, $0.295N_1$ intercepts of size l_2,..... $0.013N_1$ intercepts of size l_8. Similarly, grains of size D_2 will contribute $0.365N_2$ intercepts of size l_2, 0.295 intercepts of size l_3.........$0.005N$ intercepts of size l_8.Going down the distribution ,grains of size D_8 will contribute only $0.365N_8$ intercepts of size l_8. Thus the resulting two-dimensional distribution n_1,n_2,n_3.......n_8 is a product of the two matrices shown in equation 1:

Table 2.1 : Intercept length distribution for a tetrakaidecahedral grain model

Relative Size Range	0.0-0.13	0.13-0.18	0.18-0.24	0.24-0.30	0.30-0.42	0.42-0.56	0.56-0.75	0.75-1.0
%	1.3	0.5	2.6	4.7	8.3	17.6	29.5	36.5

$$
\begin{bmatrix} n_1 \\ n_2 \\ n_3 \\ n_4 \\ n_5 \\ n_6 \\ n_7 \\ n_8 \end{bmatrix} = \begin{bmatrix} .365 & .295 & .176 & .083 & .047 & .026 & .005 & .013 \\ 0 & .365 & .295 & .176 & .083 & .047 & .026 & .005 \\ 0 & 0 & .365 & .295 & .176 & .083 & .047 & .026 \\ 0 & 0 & 0 & .365 & .295 & .176 & .083 & .047 \\ 0 & 0 & 0 & 0 & .365 & .295 & .176 & .083 \\ 0 & 0 & 0 & 0 & 0 & .365 & .295 & .176 \\ 0 & 0 & 0 & 0 & 0 & 0 & .365 & .295 \\ 0 & 0 & 0 & 0 & 0 & 0 & 0 & .365 \end{bmatrix} X \begin{bmatrix} N_1 \\ N_2 \\ N_3 \\ N_4 \\ N_5 \\ N_6 \\ N_7 \\ N_8 \end{bmatrix}
$$

Hence , three dimensional distributions by post multiplication of the latter by the inverse matrix. For computational reasons, the two dimensional intercepts should be classed in groups .75 to 1, .56 to .75.........0 to .13 of the maximum measured intercept length·

2.1.2 Estimation of Grain Boundary Energy Distribution

Figure 2.1 shows the TEM micrographs of EGBDs. The schematic arrangement of EGBDs at the grain boundaries (during deformation) is shown in figure 2.2(a). Figure 2.2(b) shows a magnified arrangement of EGBDs at a particular boundary and pile up of discolations. At sufficient high temperatures the EGBDs can be annihilated by the process of climb , under the influence of their interacting stress fields, towards the triple point. Several investigators have measured grain energy by studying the spreading and disappearance kinetics of extrinsic grain boundary discolations (EGBDs) in the TEM during in-situ annealing. However, the techniques is cumbersome as well as prone to error in the estimation of temperature and time disappearance of EGBDs. In the traditional thermal groove method the original structure of boundaries may undergo change. Also the technique is limited to surface grain boundaries and may not be representative of the bulk material. The grain boundary energies can be simply related to the true dihedral angles between grain boundary planes in the three dimensional structure of polycrystals. Singh [16,17] has developed a technique for the estimation of the distribution of true dihedral angles from a distribution of plane dihedral angles (i.e. angles between grain boundary segments in a polycrystalline microstructure). Figure 2.3 shows threegrain boundaries, with energies γ_1, γ_2 and γ_3 meeting at a triple edge. The angles (denoted as true dihedral angles),α_1, α_2 and α_3 are the angles between the grain boundary planes in 3-dimensional structure of polycrystals. β_1, β_2 and β_3 are the corresponding plane dihedral angles between grain boundary segments. The true dihedral angles and the energies are related by the well known equation:

$$\frac{\gamma_1}{\sin \alpha_1} = \frac{\gamma_2}{\sin \alpha_2} = \frac{\gamma_3}{\sin \alpha_3} \qquad (2.2)$$

In a polycrystalline microstructure, the plane dihedral angles are the angles at the triple points, as indicated in figure 2.4. It is clear from figure 2.3.that the plane dihedral angles are not only a function of true dihedral angles but also depend on
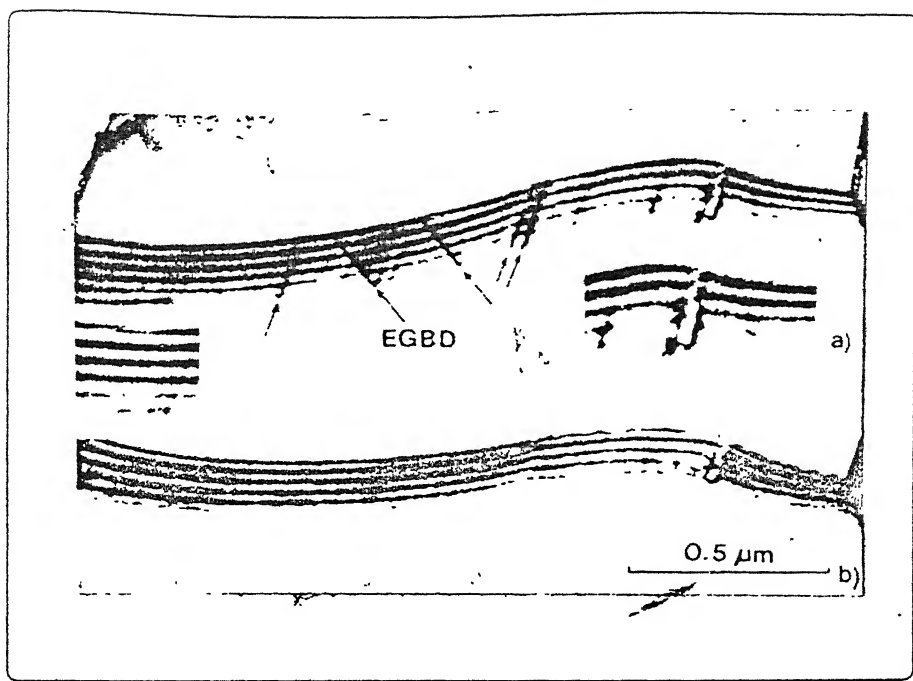
Figure 2.1 : TEM micrographs : (a) showing EGBDs at grain boundary, (b) after annealing in situ , EGBDs have disappeared
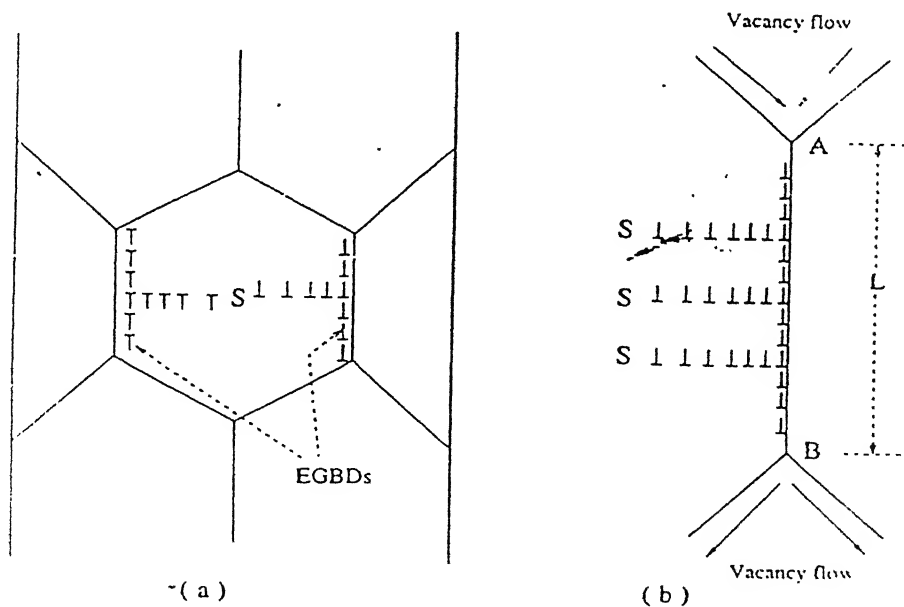
Figure 2.2 : A schematic of (a) pile –up of discolations and accumulated EGBDs at grain boundaries, (b) pile-ups and process of annihilation of EGBDs through vacancy flow at a grain boundary segment.
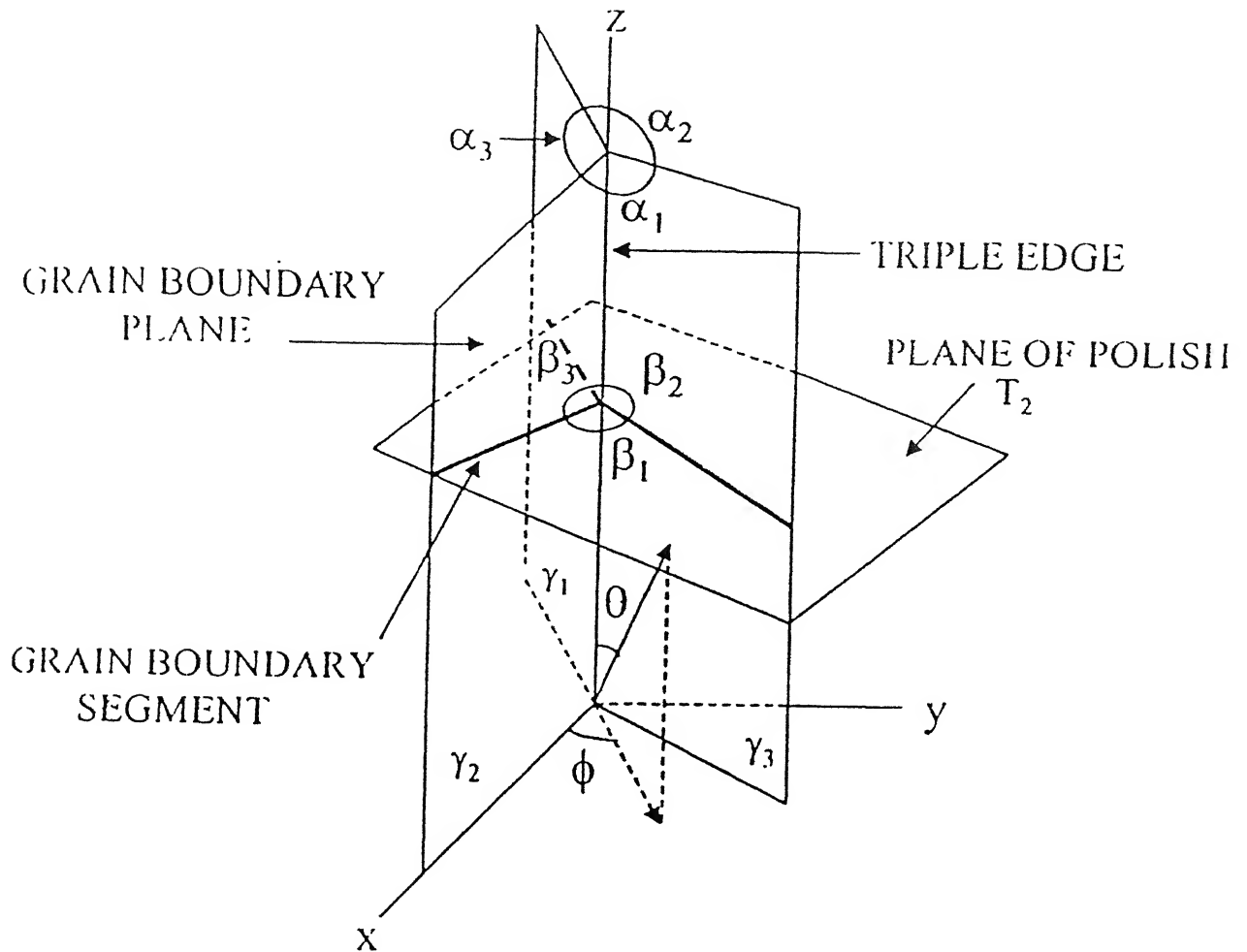
Figure 2.3 : Sectioning of a triple edge by a plane of polish randomly oriented at (θ, ϕ). α_1, α_2, and α_3 are the true dihedral angles and β_1, β_2 and β_3 are the corresponding plane dihedral angles: γ_1, γ_2 and γ_3 are the energy per unit area of the grain boundary planes.

the orientation of the sectioning plane which is defined by the orientation (θ, ϕ) of the plane normal with respect to the triple edge.

2.1.2.1 Transformation of Plane Dihedral Angles Distribution

The relationship between plane dihedral angles $(\beta_1, \beta_2$ and $\beta_3)$ and the corresponding true dihedral angles (α_1, α_2 and α_3) are given by [16,17] (see figure 2.3)

$$\cos\beta_1 = \frac{\cos^2\theta\cos\alpha_1 + \sin^2\theta\cos\phi\cos(\phi-\alpha_1)}{\{(1-\sin^2\theta\sin^2\phi)(1-\sin^2\theta\sin^2(\phi-\alpha_1))\}^{1/2}} \qquad (2.3a)$$

$$\cos\beta_3 = \frac{\cos^2\theta\cos\alpha_3 + \sin^2\theta\cos\phi\cos(\phi+\alpha_3)}{\{(1-\sin^2\theta\sin^2\phi)(1-\sin^2\theta\sin^2(\phi+\alpha_3))\}^{1/2}} \qquad (2.3b)$$

And $\qquad \beta_1 = 2\pi - (\beta_1 + \beta_3)$ $\qquad\qquad\qquad\qquad$ (2.3c)

On sectioning the polycrystalline structure (denoted as set X), the probability of an intersection of a triple edge (denoted as set Y) with the sectioning plane (denoted as set T_2) is given by [16,17] (see figure 2.5)

$$P_1(T_2 \cap Y \; T_2 \uparrow X) = \frac{2l}{\pi} \qquad\qquad\qquad (2.4)$$

where, l is the mean length of a triple edge.

He has considered a set Y_α consisting of pairs of intersecting planes making equal angles α distributed in the polycrystalline space. The intersection of Y with the sectioning plane, T_2 will give rise to a probability distribution of plane dihedral angles given by p(β /α)dβ. Let the numerical density of the set Y_α be N_v (α)dα, i.e. , number of plane pairs making an angle of α per unit volume. The probability density, g(β) of plane dihedral angles is given by:
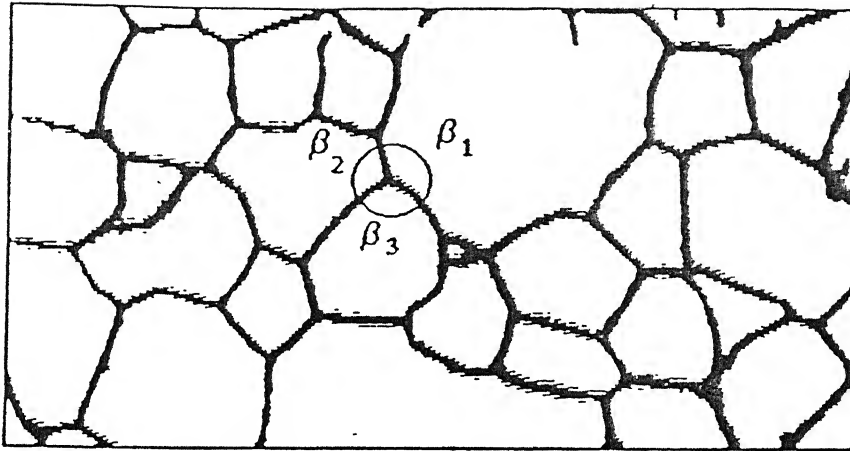
Figure 2.4 : An optical microstructure of a polycrystalline material β_1, β_2 and β_3 are the plane dihedral angles at a triple point.
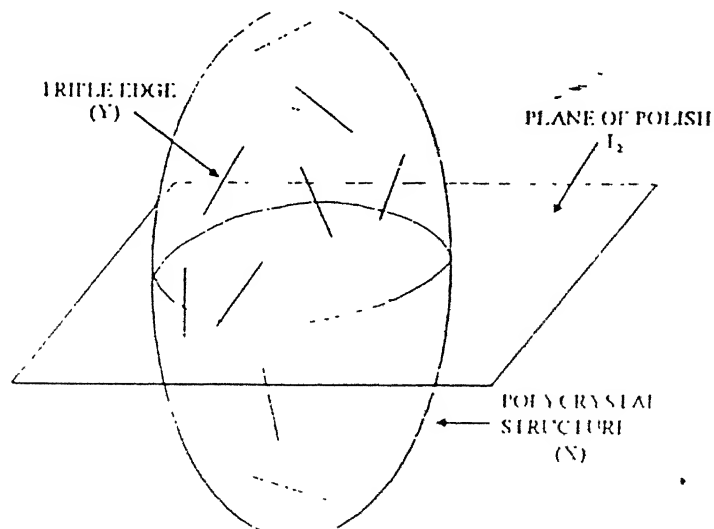
Figure 2.5 : A polycrystalline structure (X) consisting of randomly oriented triple edges being sectioned by the plane of polish(T_2)

$$g(\beta) = \frac{\int_\alpha P(T_2 \cap Y_\alpha / T_2 \uparrow X)p(\beta/\alpha)N_v(\alpha)d\alpha}{\int_\alpha P(T_2 \cap Y_\alpha / T_2 \uparrow X)N_v(\alpha)d\alpha} \qquad (2.5)$$

substituting $P(T_2 \cap Y_\alpha | T_2 \uparrow X)$ from equation (2.4), the probability density $g(\beta)$ reduces to :

$$g(\beta) = \int_\alpha p(\beta\,\alpha)f(\alpha)d\alpha \qquad (2.6)$$

where , $f(\alpha) = NV(\alpha) / \int \alpha NV(\alpha)d\alpha$ is the probability density of true dihedral angles. Equation (2.6), which is an integral equation , relates the plane dihedral angle distribution to the true dihedral angle distribution. In order to solve equation (2.6), it is discretisized by considering discrete distributions of plane as well as true dihedral angles. Both the distributions are divided into several classes. The integral equation (2.6) is converted into a set of simultaneous equations:

$$\begin{bmatrix} g_1 \\ g_2 \\ \vdots \\ g_J \\ \vdots \end{bmatrix} = \begin{bmatrix} p_{11} & p_{21} & \cdots & p_{i1} & \cdots \\ p_{12} & p_{22} & \cdots & p_{i2} & \cdots \\ \vdots & \vdots & \vdots & \vdots & \vdots \\ p_{1j} & p_{2j} & \cdots & p_{ij} & \cdots \\ \vdots & \vdots & \vdots & \vdots & \vdots \end{bmatrix} \begin{bmatrix} f_1 \\ f_2 \\ \vdots \\ f_i \\ \vdots \end{bmatrix}$$

where , g_j is the frequency of the jth class of plane dihedral angles; f is the frequency of the ith class of true dihedral angles; and p is the probability of generating a plane dihedral angle in the jth class from a true dihedral angle in the ith class. A Monte-Carlo procedure has been developed for the estimation of coefficient p_{ij} . For different class widths, a new sat values for these coefficient has to be calculated. The frequencies g_j can be determined by the measurement of plane dihedral angles on the polycrystalline microstructures. Now the frequency of true dihedral angles can be calculated by solving the simultaneous equations given in relation (2.7).

2.1.3 Concept of Fractals

Fractals are the concern of a new geometry, which provides us with a new tool to describe the geometry of nature. Natural shapes like particles, grains dendrites fracture surfaces etc. formed as a result of natural forces often defy the description of ecclidean concepts of length, depth and thickness [8] Quantitative measurement of microstructures such as perimeter, area and volume fractions cannot produce meaningful results if the principle of conventional euclidean geometry is applied.

In order to quantify these irregular natural occurring shapes and their distribution a new idea was evolved which is known as fractal dimension. We generally believe that space has 3 dimensions, a plane has 2 dimensions , a line has 1 dimensions and a point has a zero dimension.Consider an example of acricket ball with its outer shell removd.Now what is its dimensions? Surprisingly the answer depends on the observer's prospective. A far away observer will perceive it as a point and therefore to him it has a zero dimension. When the observer moves a little closer that ball seems to occupy space and therefore the dimension become 3. A still closer observer will see the interwinged strings leading one to conclude that it has a dimension 1. An even closer observer would notice that the strings are actually 3 dimensional twisted cylindrical objects. Now moving from macroscopic perspective to microscopic perspective, the 3 dimensional strings resolve into one dimensional fibres which make up the strings, and higher magnification would eventually take it to a zero dimensional atomis structure. In figure 2.6 the scenario of this changing dimension is explained.

Though the above description shows that the numerical dimension of an object may vary relative to an observer's position, there is no short boundaries where the cricket ball will change its dimension from 3 to 1 and finally to zero. Thus the idea of dimension to be only 0, 1, 2 and 3 should be abandoned and accept the inconceivable notion that dimensions can also be fractional . The fractional

dimension is called fractal dimension and it is a powerful tool in the description of complex irregularities in real microstructures of materials.

In the above context , the perimeter of the profile is meaningless as a variable in a metallurgical process. A much more meaningful parameter is the fractal dimension which is defined in the following manner. The plot shown in figure 2.7 can be represented by the following equation given below;

$$P = F\lambda^{1-D} \tag{2.8}$$

where P is perimeter, F is equal to the number 'n', of segment of length 'λ'. Here 'D' is called as the fractal dimension. For smooth euclidean /profiles the value of fractal dimension D will lie between 1 and 2.The difference between the topological dimension (1 for curves/profiles) describes the ruggedness of profile.

Figure 2.8 illustrates that the fractal dimension can characterize the degree of ruggedness of a system. A more rough system of lines or profiles will have a higher value of D. It also reflects the plane filling efficiency of a curve or a profile. A profile with large D will fill 2 dimensional space more effectively than a profile with low value of D.

The above concept of fractal dimension applied to curves can also be extended to surfaces [10]. A rugged surface will have a fractal dimension between 2 and 3, and it has a very important implication on the study of fracture surfaces as well as porous materials.

2.1.3.1 Methods of measuring Fractal dimension

The fractal dimension 'D' is a single value which is used to define fractal image [10,14]. Two different fractal images can have same fractal value 'D'. For the images consists of lines the 'D' value lies between 1 and 2 and for planes the 'D' value lies between 2 and 3. There are two techniques for measuring the fractal dimensions of grain boundaries.

Far Observer
(0 Dimension)

Moves Closer
(3 Dimension)

Still Closer Observer
(1 Dimension)

Near Observer
(2 Dimension)

Nearer Observer'
(1 Dimension)

Microscopic View
(0 Dimension)
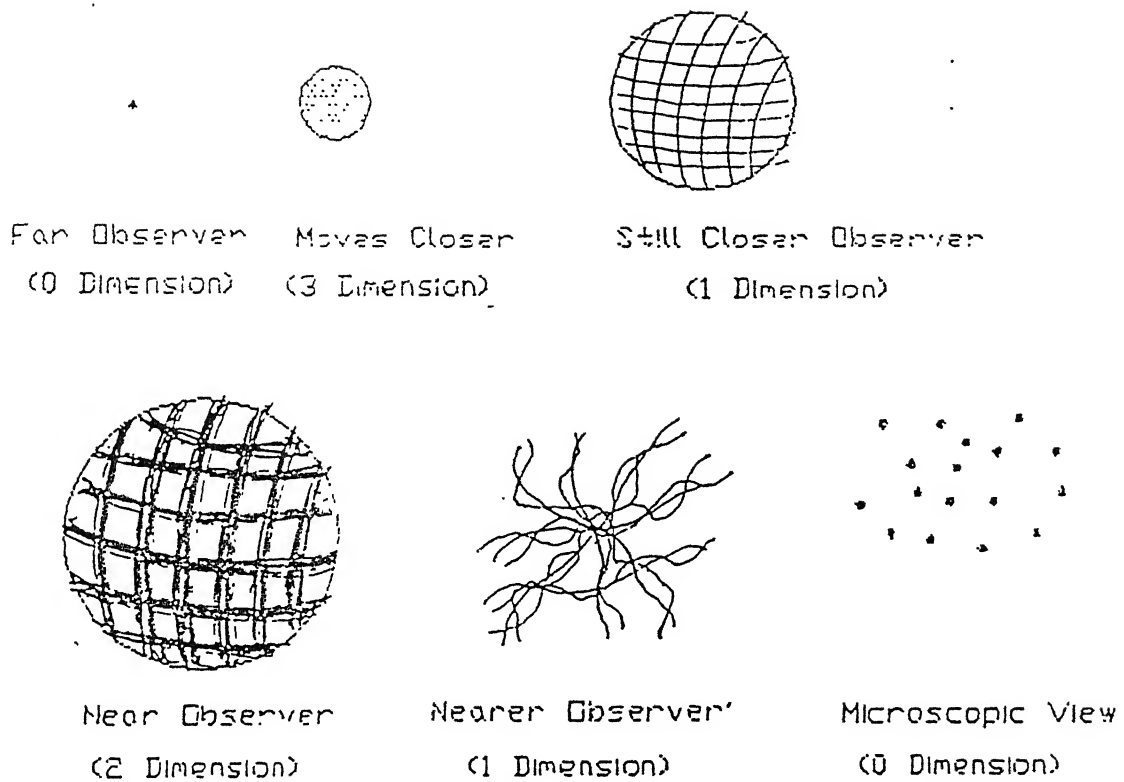
Figure 2.6 : An observers perspective of the changing fractal dimension for cricket ball with its shell removed.
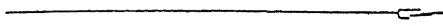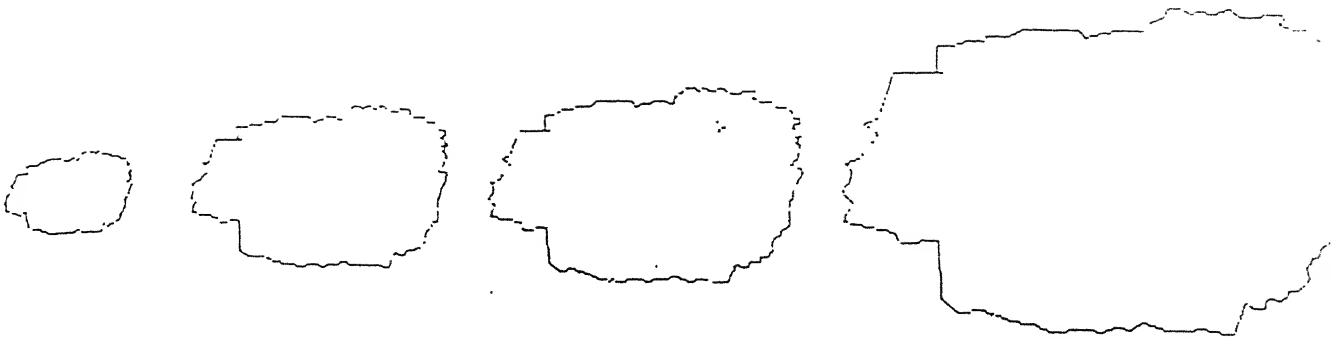
Series of Magnified Views

PLOT OF PERIMETER VERSUS STEP SIZE

SLOPE = 1 − D,   D = 1.3
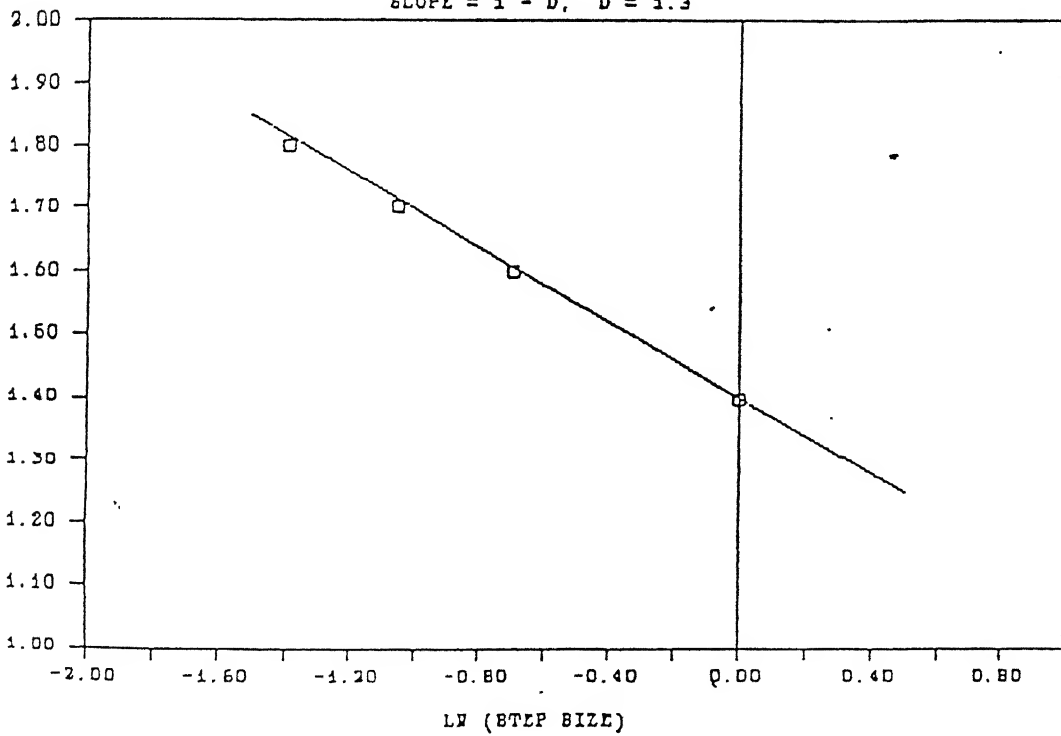
LN (STEP SIZE)

Figure 2.7 : A particle viewed at increasing magnification, perimeter of the particle plotted as the function of the step size λ

2.1.3.1.1 Box Technique

This method uses different sizes of square grids to obtain fractal dimension [8,9]. A square grid of size 'δ ' is placed over the microstructure (figure2.9) and then the number of square grids overlap the grain boundaries are counted. This process is repeated for different values of 'δ ' in the plot of log(N) vs. log(δ) the slope gives the value of ' –D'.

$$N = K\delta^{-D} \qquad (2.9)$$

where K is a constant.

2.1.3.1.2. Divider Technique

A divider or yardstick of certain length is chosen and straight line segments are cut-off along the grain boundaries [13] and count the number straight line segments 'N' (to fully cover the grain boundaries)

$$L = N.\delta \qquad (2.10)$$

And $\qquad L = K.\delta^{1-D} \qquad (2.11)$

from the plot log(L) vs. log(δ) the slope will give '1-D'.

Two basic approaches have been used to analyze the fractal character of fracture surfaces.

2.1.3.1.3 Slid Island Technique

The perimeters and area's of 'islands' (which are typical of fracture surface) are measured to obtain the fractal dimension [14]. This technique, originally described by Mandelbrot et.al.[10] is based on the perimeter area relationship of the islands produced by horizantal sectioning of the surface.

Topological Dimension		Fractal Dimension
I		1 00
I		1.02
I		1.25
I		1.45
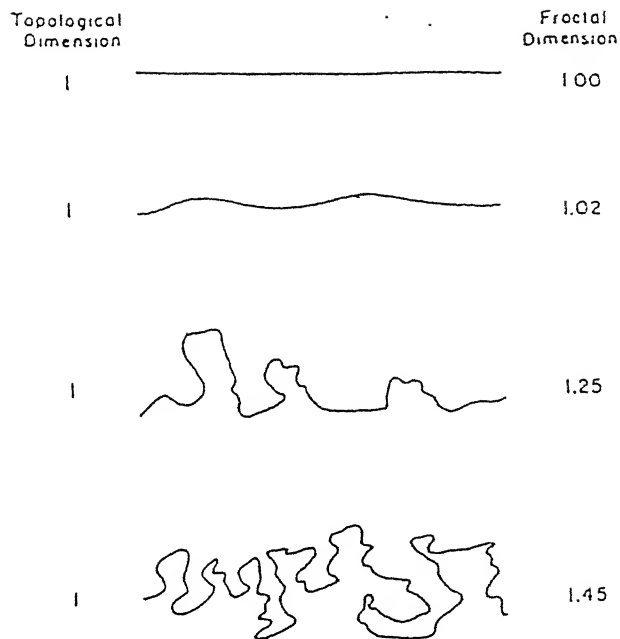
Figure 2.8 : An illustration of the use of fractal dimension as a parameter in characterizing the roughness or ruggedness of lines.
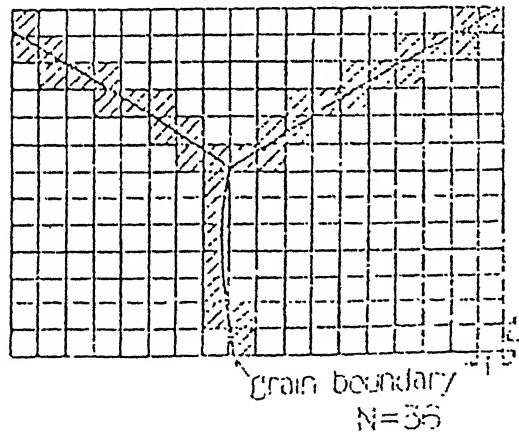
grain boundary
N=36

Figure 2.9 : A schematic of procedure to obtain the fractal dimension of grain boundaries in a photograph (N is the no.of squares intersected with grain boundaries and r is the size of the square). N is 36 in this case

It is known that the perimeter-area relation is often of the form of;

$$\log P_I(\varepsilon) = C_I + D_f/2 \log A_I(\varepsilon) \qquad (2.12)$$

Where 'D_f' is the fractal dimension and $D_f/2$ is the slope of the straight line in a log-log diagram of perimeter vs. area (figure 2.10). A_I and P_I Are the perimeter and area of the islands measured with constant yardstick length 'ε' of the i [th] island. The fractal dimension of the coastline is given by $D_f - 1$

This method may yield incorrect result as a fractal dimension if the islands are not exactly the same as each other [12]. The result may be correct if the islands have the same C_I s, for example are of similar shape, and may be incorrect if they have different C_i s. If the D_f of a surface obtained by SIM is between 1 and 2,one cannot decide whether this value is correct or incorrect.As it is very difficult to test the similarity of the islands, the applicablity of SIM is problematic.

2.1.3.1.4 Electrochemical Approach

The third approach is an electrochemical method in which the fractal dimension is measured by the diffusion limited current on the fractal like working electrode. This method is used mainly in electrochemical problems, but it is applicable in other fields as e.g. characterization of fractured steel samples.

2.1.3.2 Applications of Fractals

2.1.3.2.1 Correlation of Fractal dimension to creep properties

Effect of microstructures such as grain size and grain configuration and creep conditions on fractal dimension of the grain boundary fracture surface was examined by manabu Tanaka [8,11] using several heat resistant alloys of nickel, cobalt and iron base under various stresses in the temperature range from 973 to 1422k.

He observed that fractal dimension of the grain boundary fracture increases slightly with decreasing grain size, since the number of grain boundary

microcracks which were linked to the fracture surface increased with decreasing grain size. The fractal dimension of the grain boundary fracture in the spacimens raptured increased with decreasing creep stress. This behaviour was correlated to the stress and temperature dependence of the grain boundary sliding which control the initiation and growth of grain boundary microcracks and the oxidation during high temperature creep.

He also observed that both the rapture strength ratio and rapture ductility ratio of specimens with serrated grain boundaries to those with straight grain boundaries increased with increase of the fractal dimension difference of grain boundaries of these specimens.

2.1.3.2.2 Application of Fractals to Fracture Processes

Fracture surfaces produced as a result of external loading usually rough and irregular and experimental evidences are there which suggests that they are fractal in nature. An example of the correlation between fractal dimension of fracture surfaces and impact energy is shown in figure 2.11. This shows that the fractal dimension decreases linearly with increasing impact energy.Q.Y.Long et.al.[15]

Studied the fractal dimension of fracture surface created by sterss corrosion cracking in high strength steels. He observed that the fractal dimension of different locations of fracture surfaces corresponding to the sub-critical propagation zone of stress corrosion cracking varies positively with the local stress intensity factor K_1 ahead of the crack tip and increases as the crack grows. Therefore during the process of stress corrosion cracking fractal dimension increases.Xing-Gang Jiang et.al. determined the relationship between 'J $_{Ic}$' and fractal value of fracture surface of ductile materials. He got the following result;

$$J_{IC} = \frac{\sigma_o}{3} \ln(\frac{4^{1-D_F^{-1}} - 1}{12f_p})l_o^*$$
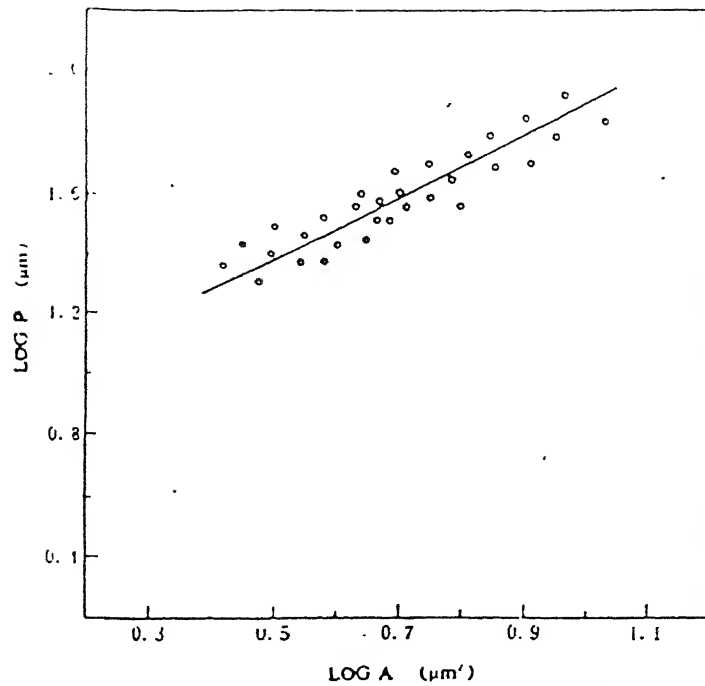
Figure 2.10: A typical example of perimeter P vs. area A of ferrite in ferrite-martensite steel showing the linear variation of log P with log A.
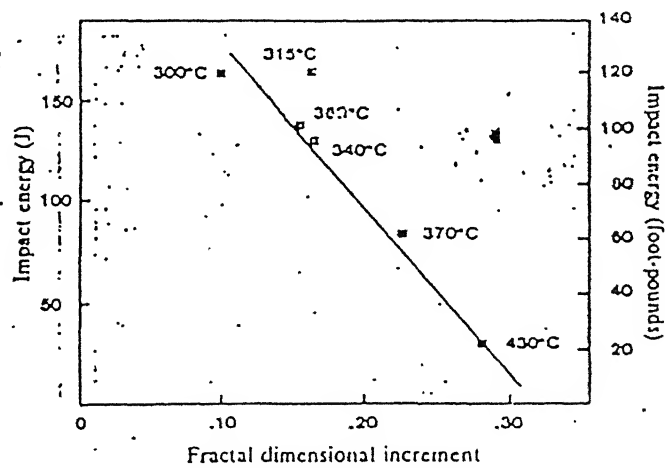
Figure 2.11 : Room temperature impact energy vs. fractal dimension in 300 grade maraging steel.

where σ_o is the tensile strength of the material

  f_P is the volume fraction of void initiating particles

  l_o^* is charactreistic distance

The formula shows that the higher the value of the fracture surface ,the larger the J_{IC}

2.2 An Introduction To Texture In Metals.

The common metals of industrial practice are polycrystalline aggregates in which each of the individual grains has an orientation that differs from those of its neighbours. It is quite unusual for the grains in such metals to have a random distribution of orientation, and the non random distributions that occurs are called preffered orientations or textures [19].

Textures are developed at all stages of the manufacturing process of matals, but the precise nature of texture is a complex function of of the mechanical and thermal treatments as well as the material itself. The important processing factors can be discussed qualitatively under four broad categories, viz. solidifaction, deformation, annealing and phase transformations. Texture may consist of one component or many component.

2.2.1 Description and Respresentation of Texture

The crystallographic texture in a rolled polycrystalline material is usually represented as {hkl}<uvw> where (hkl) represents the set of planes of the crystal that are parallel to the rolling plane and <uvw> represents the set of directions that are along the rolling direction. This is shown in figure 2.12. Texture in a specimen may consist of a number of components and it is generally reported in the form of pole figures [19].

Pole figures are simple stereographic projections which show the distribution of particular crystallographic directions in the assembly of grains that constitute the metals. Pole figures must contain some reference directions and these are usually chosen so that they correspond to easily defined directions in the specimen.In rolled sheet for example it is natural to think in terms of the rolling directions (RD), the transverse direction (TD), and the sheet plane normal (ND). Figure 2.13(a) shows how the sheet is considered to sit at the centre of the steregraphis sphere with the orthogonal reference directions as x, y and z axes. The orientation of a single grain in the sample can be represented by plotting its three {100} poles at the appropriate angular positions relative to the reference directions. In practice all the concerned are projected on to the equatorial plane to produce a stereographic projection as shown in figure 2.13(b). The result is a pole figure,in this case a (100) pole figure, showing the positions of the {100} poles for the grains and, therefore, the orientation of the grain in the sheet.

For a polycrystalline sample all the grains must be considered and three {100} poles must be plotted for each to give the pole figure. If the resulting poles are distributed uniformly over the area of projection there is no preffered orientation and the specimen is said to have a random texture. In real metals this condition is most uncommon and the poles tend to cluster together in certain areas of the pole figure to produce a texture as shown schematically in figure 2.13(c). The number of grains is normally such that the determination of individual orientations is impractical and the plotting of individual poles impossible. To overcome these difficulties it is usual to collect data from many grains simultaneously and to represent this in the form of density contours on the pole figures. Figures 2.13(d) and 2.13(e) show how the pole density may be visualised and presented as contour lines on the steregraphic projection. The density values are expressed relative to that which would be expected for a specimen having a random orientation. Contour levels greater than 1x random imply a concentration of poles and those less than 1x random adepletion in the direction concerned.
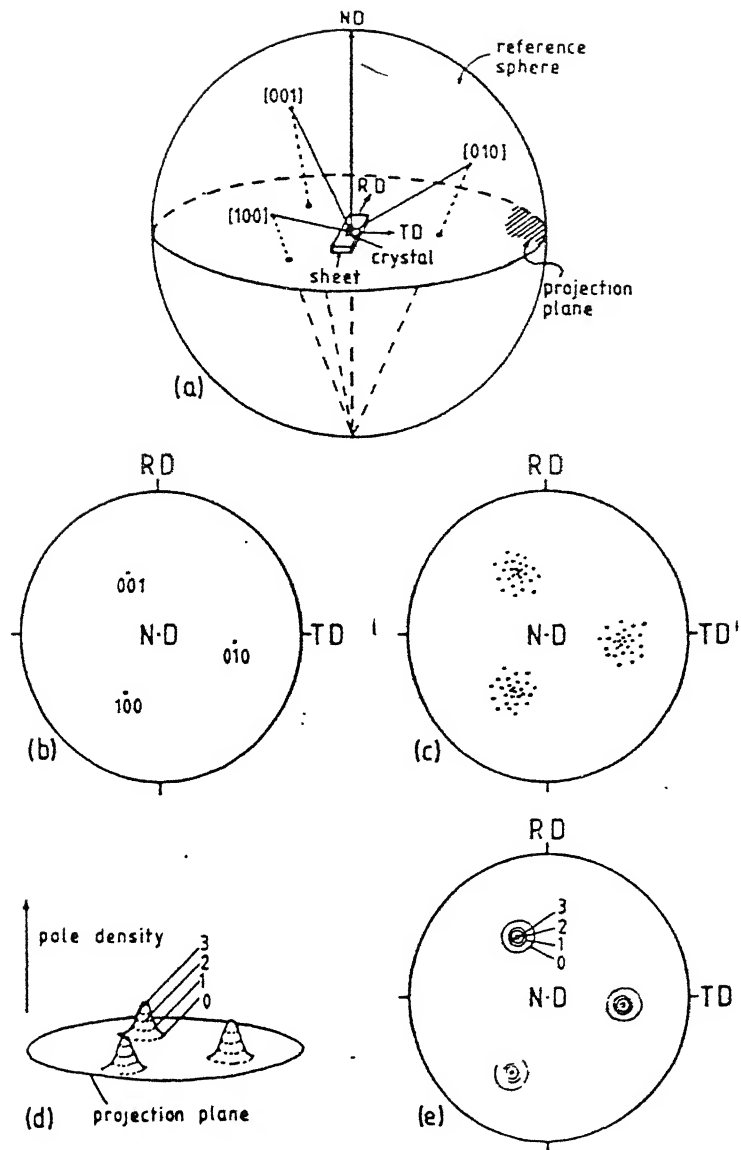
Figure 2.13 : (a) Projection sphere and reference directions, (b) Projection of poles for a single grain, (c) Projection of poles from textured grains, (d) Pole density distribution, (e) contour map of pole density.

But, a better way of representing texture is through the use of Orientation Distribution Function (ODF) [19], which provides a more quantitative description of texture than a pole figure. An ODF describes the frequency of orientations in three dimensional orientation space (Euler space) which is defined by the three euler angles ϕ_1, ϕ and ϕ_2. These are three consecutive rotations which transforms the specimen frame S to the crytallographic frame C as shown in figure 2.14. Any particular texture component {hkl}<uvw> can be completely represented by a point (ϕ_1, ϕ, ϕ_2) in the Euler space. Each texture component has a distinct position in the orientation space and as a result the quantitative analysis of texture with a much better resolution is possible using the ODF method.The schematic diagram of the Euler space is shown in figure 2.15.

The experimental pole figure data are converted to ODF through mathematical methods developed by Bunge and Roe who used spherical harmonic functions to represent orientation distribution. In the Bunge notation which is more commonly used in texture study the orientation space is defined by three orthogonal axes ϕ_1, ϕ, ϕ_2 each ranging from $0°$ to $90°$. This total volume is divided into three basic ranges in which each orientation appears only once. The value of the orientation density at each point is the intensity of that orientation in multiples of the random.

2.2.2 Experimental Determination of Texture

The vast majority of texture determinations are done using the well established principles of x-ray diffraction from polycrystals although some alternative techniques such as Neutron diffraction method are occasionly used.

All the variants of the diffraction method use a monochromatic beam of radiation with the bragg condition fixed for a single set of reflecting planes and maintained throughout the determination of pole figure.under these conditions the normal (k) to the diffracting plane {h,k,l} remains fixed in space and the specimen is rotated through a wide range of angles so that many different directions in the sample are brought into coincidence with the diffracting normal.Whenever a crystal become so oriented that the normal to any one set of the prescribed {h,k,l}
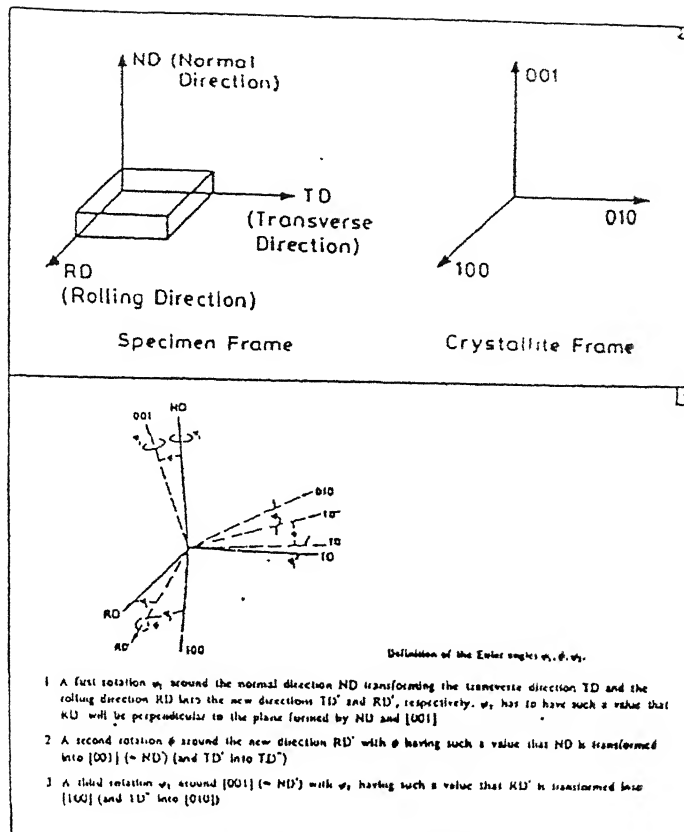
Figure 2.14 : Schematic representation of three euler angles ϕ_1, ϕ_2, ϕ_3 ; (a) specimen frame S and crystallite frame C, (b) transformation of specimen frame into crystallite frame.
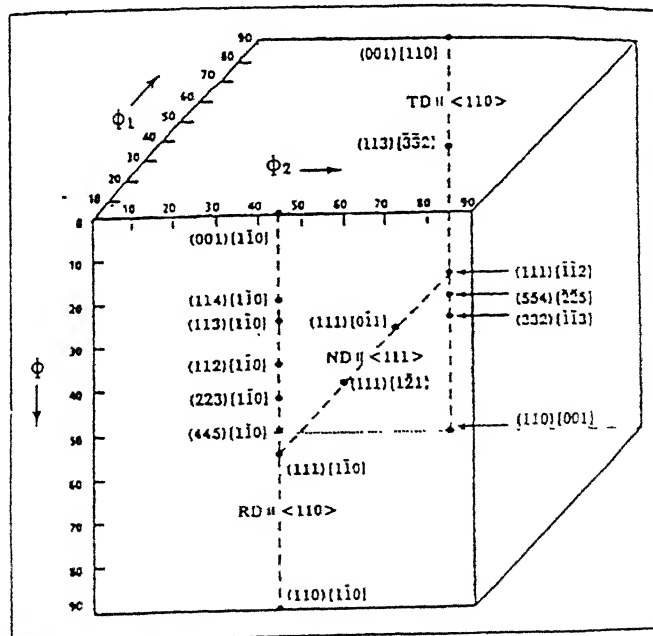
Figure 2.15 : Schematic presentation of Euler space.

planes coincides with the fixed normal, k, a diffracted intensity will be measured from that grain. The total diffracted intensity at any instant is then proportional to the volume of the specimen in which the {h,k,l} planes are so oriented. In other words, the measured intensity at a given time

Is directly proportional to the pole density on the pole figureat the position under investigation. The proportionality between diffracted intensity and pole density is usually quantified in terms of the 'Random intensity', or the intensity which is observed when a textureless sample is examined under precisely the same conditions. The pole figure is then plotted out with contour levels which correspond to ½,1,2,3,…..x random intensity.

This provides a sensible basis on which the sharpness of the texture may be assessed and allows a comparison to be made between results obtained in different laboratories and using different experimental methods.

Many techniques and variations have been proposed over the years for determining preferred orientation, such as[19]:

1 The schulz Reflection Method

2 The Transmission Method

3 The Offset Quadrant Method

4 The Spherical Specimen Method etc.

Pole figures can be achieved completely by some elaborate methods , but they are most commonly determined in an incomplete form by the Schulz reflection method [19].

2.2.2.1 The Schulz Reflection Method

When mounted on goniometer the spacimen is subjected to three types of movement. These are:

1 Simple translation to and fro which improves the statistical averaging of the texture measurement by increasing the number of grains that are sampled.

2 Rotation about an axis perpendicular to the sheet surface

3 Rotation about an orthogonal axis.

Figure 2.16(a) shows a commercial texture goniometer with a specimen in position. A schematic diagram which explains the geometrical arrangemant is shown in figure 2.16(b), and the corresponding stereographic projection is given in figure 2.16(c).

The problem that arises with the Schulz method is that the diffracted intensity is affected by the geometrical setting of the goniometer as well as by the variation in texture that is being measured.

When determining a pole figure from an unknown textured material, it is normal practise to carry out a run on a specimen which is untextured or 'Random'. This specimen serves two important purposes. Since it has no texture any variation in the measured diffraction intensity may be attributed solely to the defocussing effect and so it provides a means of correction for defocussing. Secondly, it provides a logical reference intensity level with which to compare to the textured material. Regions in the pole figure which show less than the random specimen intensity may be considered depleted in poles. The augmented intensity regions are readily quantified by contours of 2x random,3x random….etc.

Figure 2.17(a) shows a chart recording of a (111) pole figure for 95% cold rolled aluminium and demonstrates how the random sample is used in the plotting procedure. Superimposed on the texture plot is the intensity which was measured from the random sample (labelled 1x random) which shows the loss of intensity due to defocussing at the higher φ values. Also shown is the background level which is simply determined by by moving the detector arm of the goniometer a small distance from the bragg condition and recording the intensity. A series of reference lines are then drawn which represents multiples
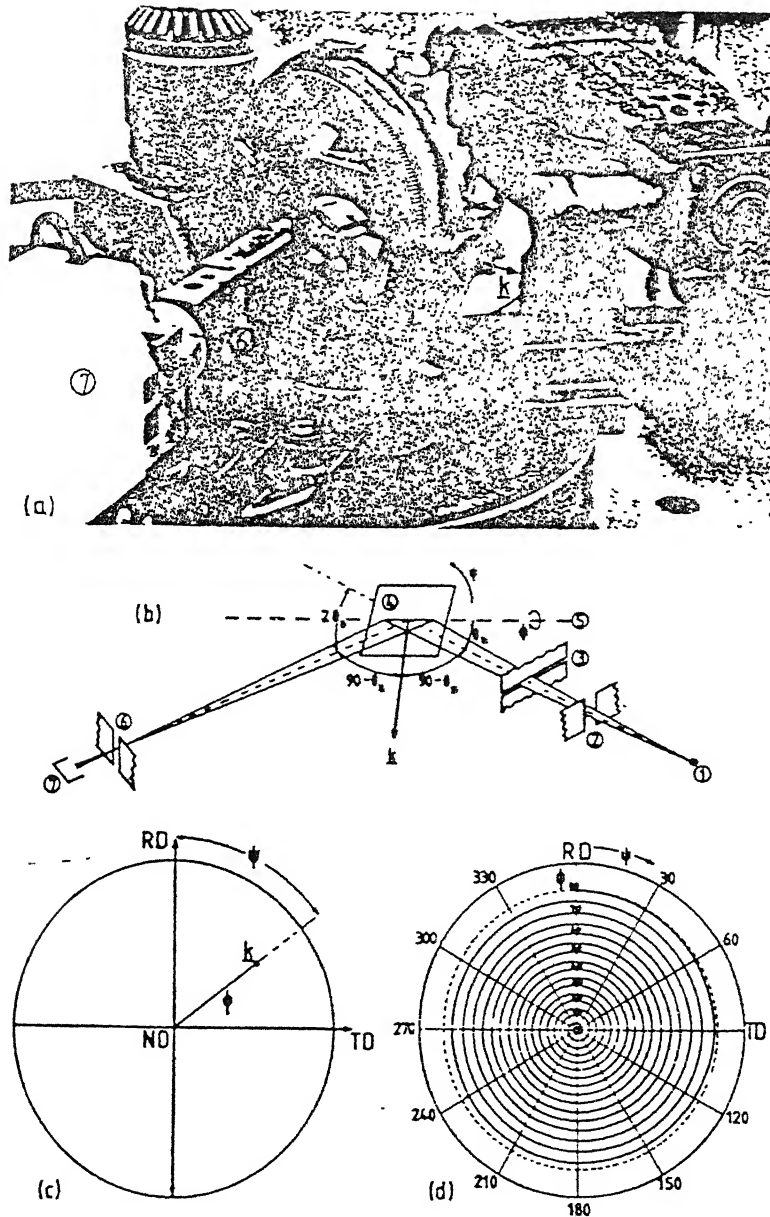
Figure 2.16 : (a) Experimental texture goniometer, (b) Schematic diagram of (a),
(c) Projection showing the diffracting vector K, (d) Spiral path of the diffracting
vector.
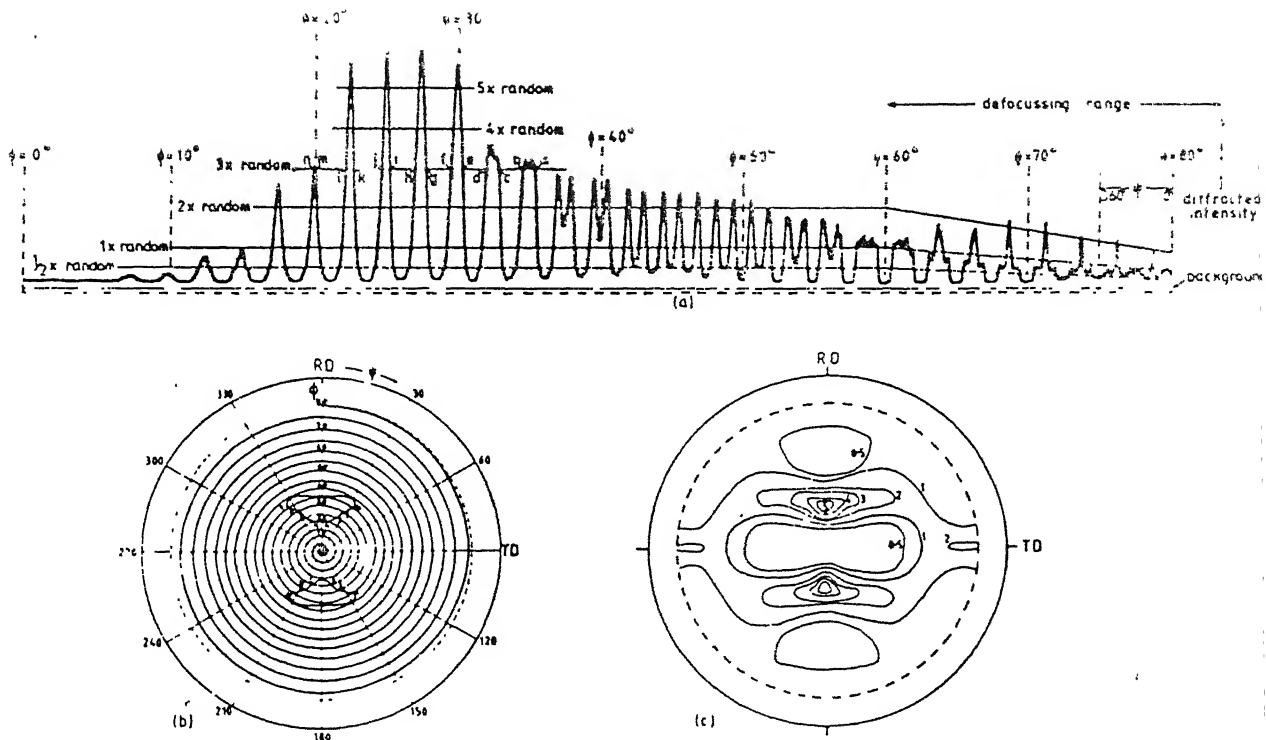
Figure 2.17 : (a) Chart recording for the (111) reflection of cold rolled aluminium (compressed scale), (b) Partly plotted pole figure showing the 3x random contour, (c) final (111) pole figure.

and submultiples of the diffracted intensity from the random sample. To determine these values the diffracted intensity (i.e.total measured intensity minus the background value) is multiplied by n for the nx random level and then the background level is added on. When plotting a contour on the pole figure; figure 2.17(b), marks are made on the spiral path at each point corresponding to the values of ϕ and ψ where the measured intensity traces cuts the particular reference line concerned. These marks are then joined to give a contour line which seperates the areas of the pole figure which are above that reference level from those which are below it. The small letters on the 3x random level in figure 2.17(a) and 2.17(b) indicate how this information is transferred from the chart to the pole figure to produce the 3x random contour. The completed pole figure is shown in figure 2.17(c). To overcome the problems of Schulz method a number of other methods and variations as mentioned above have been proposed.

Chapter 3

Experimental Procedure

3.1 Material

95%cold rolled Ni 10%Co alloy has been selected for study. The chemical composition of the alloy (wt%) is given in Table3.1. The material was in the form of a sheet. It was cut and subjected to annealing treatment. After that dihedral angles and other quantitative studies were made on the heat treated and prepared specimens. Phase diagram for the alloy is given in figure 3.1.

Table 3.1 : Composition of Ni-10%Co alloy.

Nominal composition	Detailed Composition (wt%)						
	Fe	Co	C	S	Si	Cu	Ni
Ni 10%Co	-	11.15	0.006	0.003	0.03	0.03	Balance
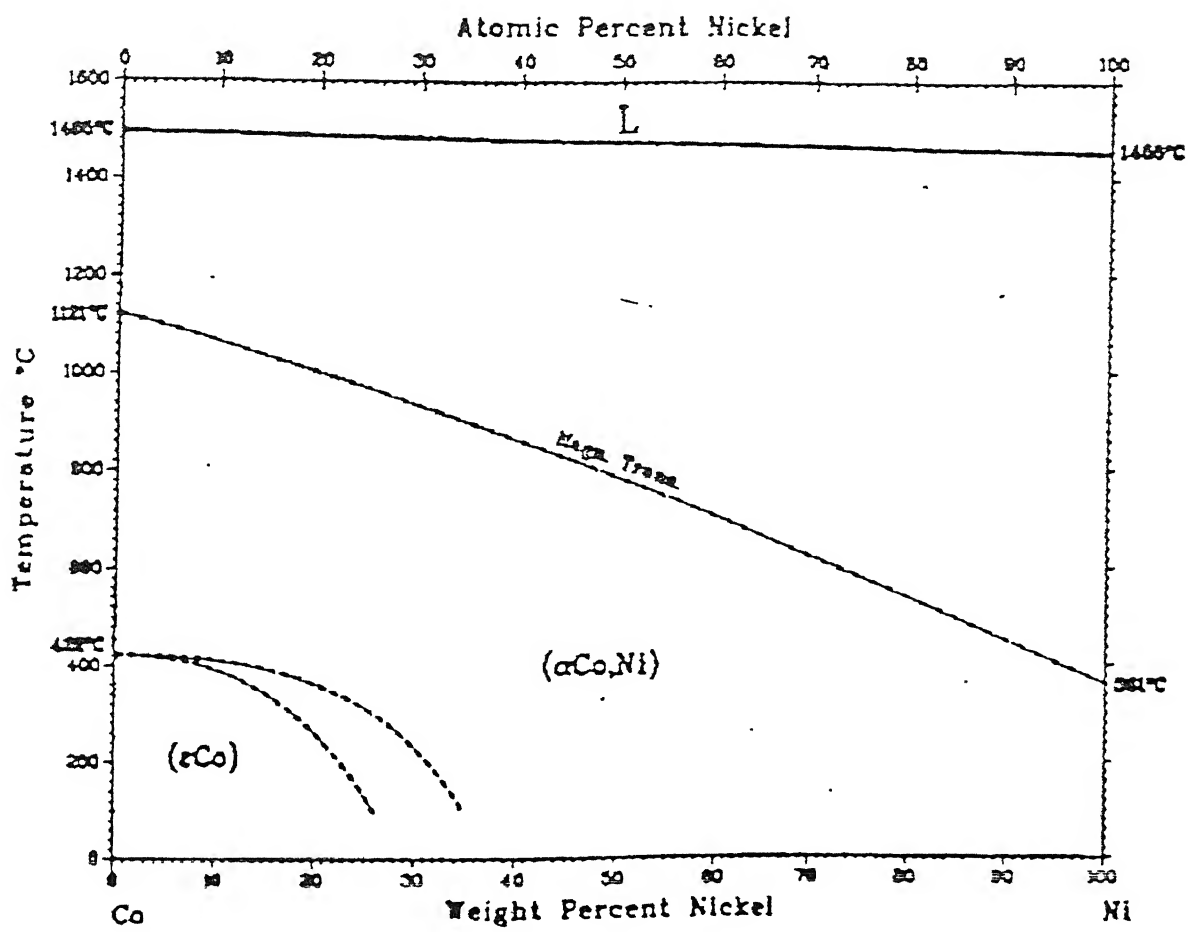
Figure 3.1 : Phase diagram of Ni-10%Co alloy.

3.2 Sample Preparation

Small pieces of size 1x1 cm of square shapes were cut from the as received 95% cold rolled strip.

3.2.1 Heat Treatment

The heat treatment was carried out in a Laboratory Tube type furnace. Five samples of square shape were each hanged with the help of five wires inside the furnace. They were annealed at 800° for five different timings of 1hour, 3hours, 10hours, 20hours and 50hours in an Argon atmosphere. Gas was continuously passed through the furnace, and finally the samples were quenched in tap water.

3.3 Microscopy

3.3.1 Samples were cold mounted for examination under the optical microscope. The samples for optical microscopy were ground and polished on emery papers (0 to 4 grades) followed by wet polish with alumina suspension of particle size 1 m to .05 m respectively. These were subsequently etched before examining the microstructure. The etching reagents used are:

-2 gm anhydrous $FeCl_3$ in 96 ml ethanol and 2 ml HCl

All the microstructures were photographed with the help of Leitz Metallux microscope having camera attachment. Photographs were taken at a magnification of 200X.

3.3.2 Quantitative Metallography

The following metallographic measurements were carried out from various microstructures. The parameters used for characterizing the microstructures are discussed in the following sub-sections.

3.3.2.1 Grain Size

The Spatial grain size distributions from linear intercept distributions have been determined using a Matrix Method, given in section 2.1. It can be seen from there that the two dimensional intercept distribution is equal to the product of two matrix given there. The inverse of the matrix is known, so the spatial grain size distribution can be easily obtained by multiplying the inverse matrix with the Matrix for intercept length distribution. A set of parallel lines of fixed spacing were used for obtaining the required Intercept length distributions. Intercept lengths were measured at two angles of $0°$ and $90°$ respectively. Measurements were taken from nearly the whole area of the micrographs.

3.3.2.2 Dihedral Angles

The plane dihedral angles i.e. the angle between grain boundary segments at the triple point on two dimensional plane polished section (shown in figure 2.4) were measured from the traced micrographs of annealed samples. Near about all the triple points were taken in to account and angle between grain boundary lines were measured. The distribution of the true dihedral angles i.e.angle between grain boundary planes at a grain edge in 3 dimension (shown in figure 2.3) was estimated from these measured plane dihedral angles using a computer programme developed on the basis of the technique discussed in section 2.2.1. Then the standard deviation of plane dihedral angles and the calculated true dihedral angles were determined. Also, an analysis discussed in section 5.2 of chapter 5 was done to obtain energy distribution for the grain boundaries.

3.3.2.3 Fractal Dimension

Fractal dimension was calculated using box technique (section2.2.1.1), which is regarded as the most accurate method for determining fractal dimension from experimental data.In this a square grid of size 'δ' was placed over the microstructures and number of squares intercepted by the grain boubdaries were

counted.This process is repeated for various sizes of 'δ' (from 10μm to 35μm).Then from the plot of log(N) vs. log(δ) the slope was calculated which gives the value of –D.

$$N=K\delta^{-D}$$

Where K is a constant and D is the fractal dimension of the grain boundary.

Chapter 4

Results

As mentioned in chapter 3, the model Ni-10%Co alloy was annealed at 800°C for five different annealing times of 1, 3, 10, 20 and 50 hours respectively and then the stereological measurements were done on the annealed samples

The parameters studied to quantify the microstructural features of the material were:

1 Grain size

2 Dihedral angles

3 Fractal dimensions

All the measured data and calculated results, in the tabular and graphical form are shown in this chapter. These parameters were than correlated with the Texture data (volume fractions and Intensity values) of {100}<001> Cube Component.

4.1 Characterisation of Microstructures in Annealed Samples:

4.1.1 Grain Size

The spatial grain size distribution was determined from linear intercepts distribution by using a matrix approach. Table 4.1 shows the different calculated parameters of intercepts length distribution and Table 4.2 presents the same for for the spatial size distribution. Figure 4.6 shows the variation of mean intercepts length (with 95% confidence interval) and figure 4.7 presents the variation of mean of spatial grain size distribution with annealing time respectively. Table 4.3 to 4.7 presents the entire analysis done for the determination of spatial grain size distribution for the five differently annealed samples. Figure 4.8 to 4.12 presents the spatial grain size distribution for the five different samples.

(a)
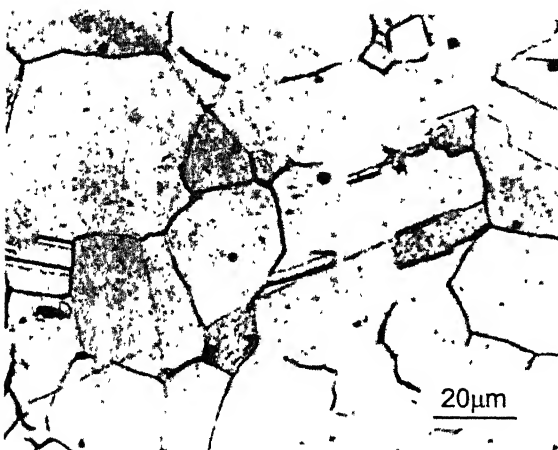
(b)
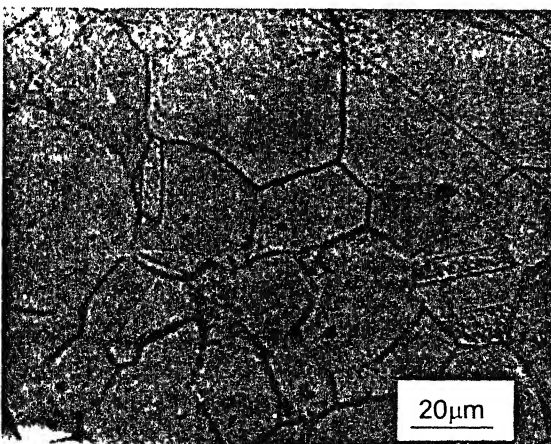
(c)

Figure 4.1 : Micrographs of 1 hour annealed sample.
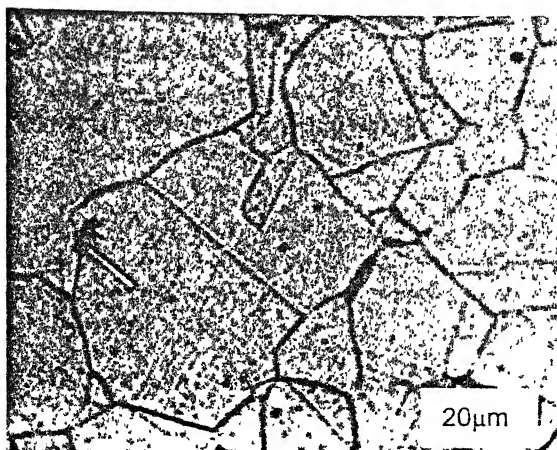
(a)
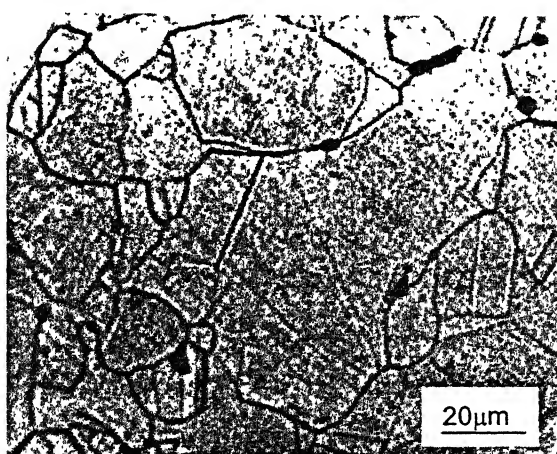
(b)
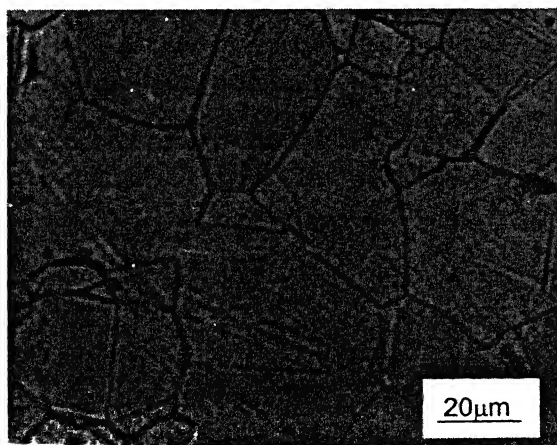
(c)

Figure 4.2 : Micrographs of 3 hours annealed sample.
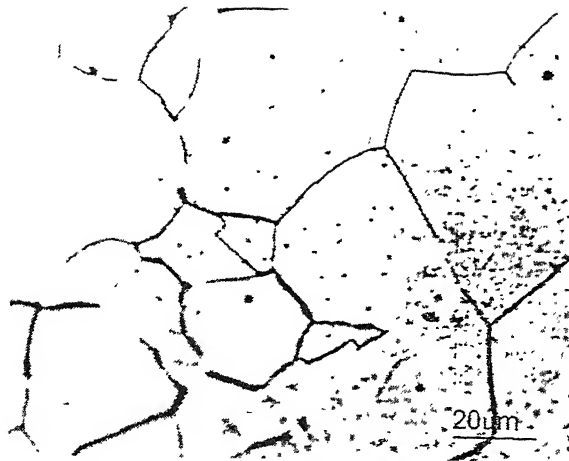
(a)
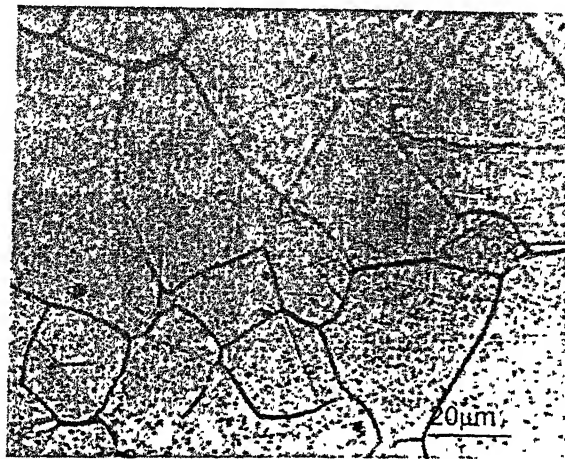
(b)
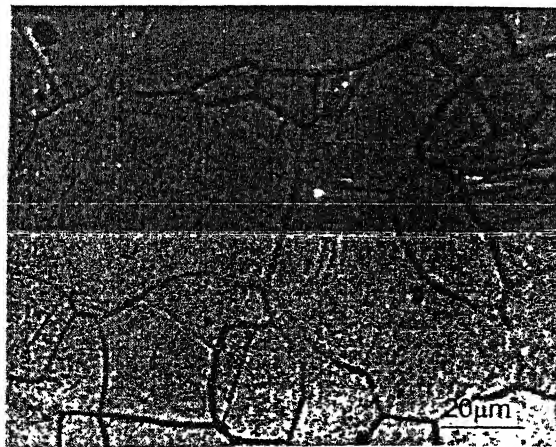
(c)

Figure 4.3 : Micrographs of 10 hours annealed sample.
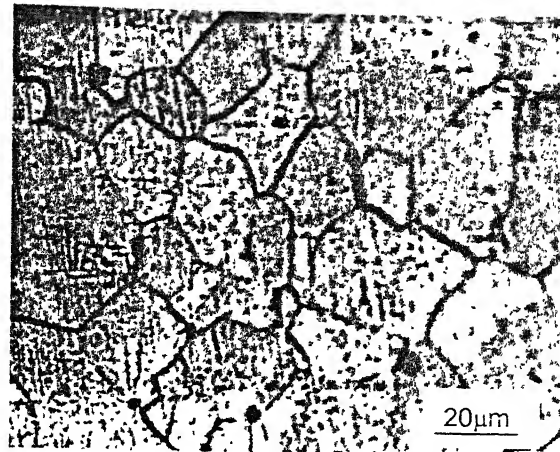
(a)
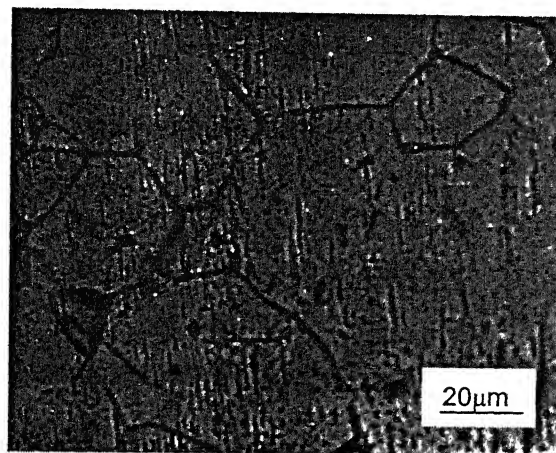
(b)
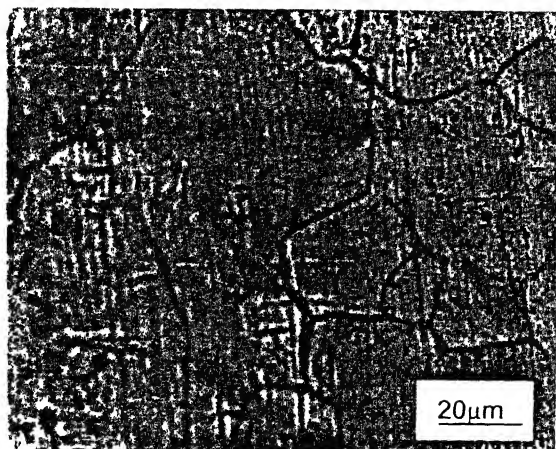
(c)

Figure 4.4 : Micrographs of 20 hours annealed sample.
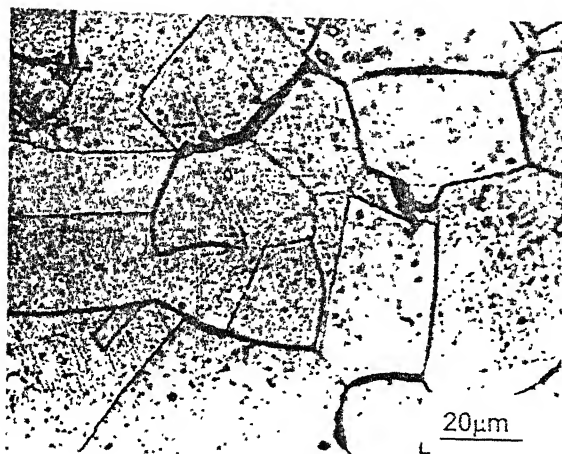
(a)
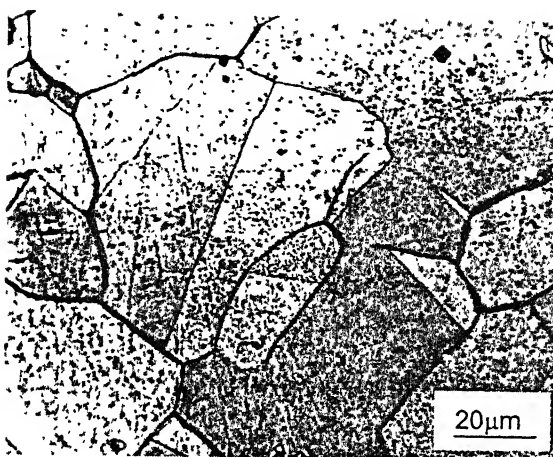
(b)
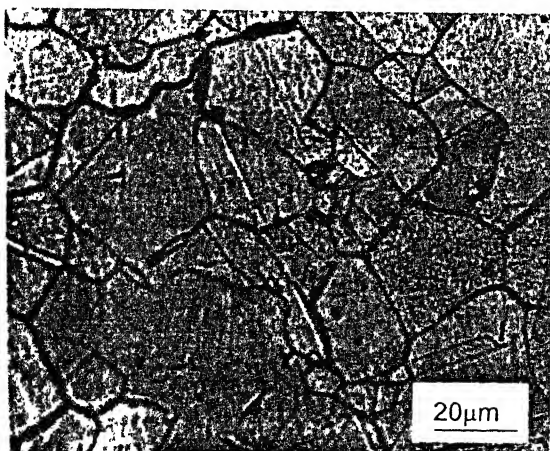
(c)

Figure 4.5 : Micrographs of 50 hours annealed sample.

Table 4.1 : Different parameters of intercepts length distribution

Annealing time (Hours)	Mean Intercept length with 95% confidence interval (µm)	Standard deviation (µm)
1	54.0±0.044	32.75
3	46.5±0.040	27.35
10	58.0±0.048	37.85
20	59.5±0.080	46.85
50	96.5±0.098	72.5

Table 4.2 : Different parameters of spatial grain size distributiom.

Annealing time (hours)	Mean grain size, µm (3D grain diameter)	Standard deviation (µm)
1	33.2	27.04
3	29.3	25.26
10	41.2	51.59
20	32.5	26.50
50	33.0	29.40
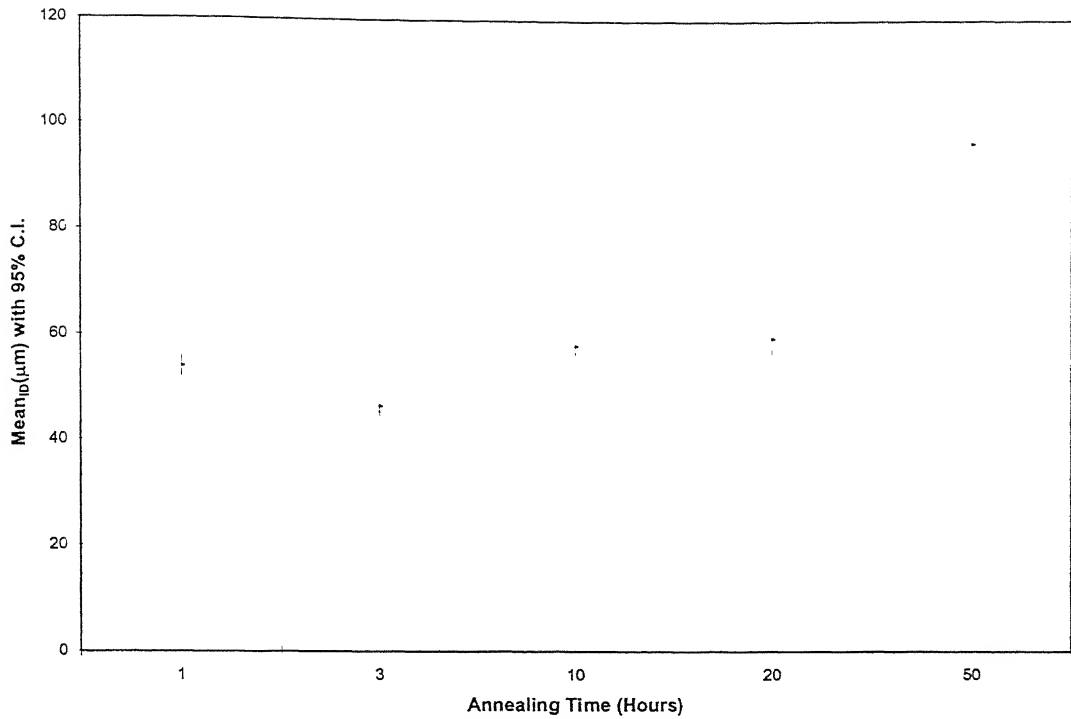
Figure 4.6 : Variation of mean intercept lengths (plotted with 95% confidence interval) of intercept length distributions with annealing time.
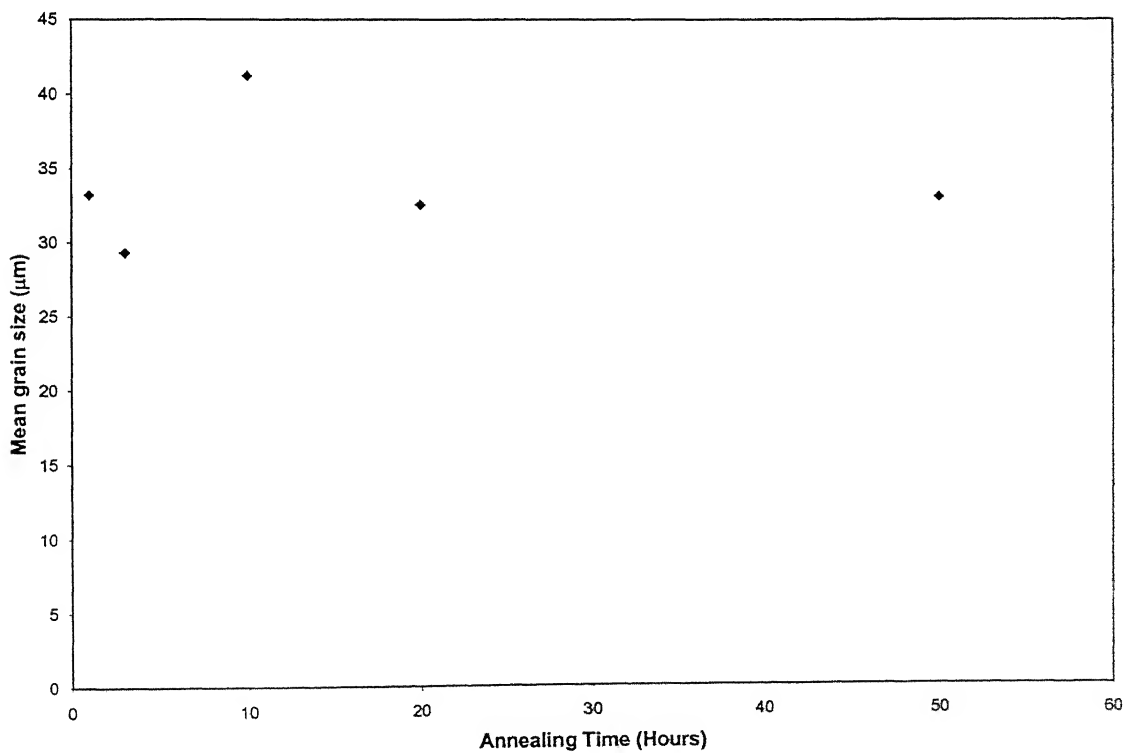
Figure 4.7 : Variation of mean grain size (of spatial grain size distribution) with annealing time.

Table 4.3 : Different frequency distributions for the determination of spatial grain size distribution for 1 hour annealed sample.

Size class interval (µm)	Relative frequencies of linear intercepts	Cumulative frequencies of linear intercepts	Normalised frequencies of 3D grain diameter (normalised after −ve values were put to zero)	Cumulative frequencies of 3D grain diameter.
0.0-30	0.334	0.334	0.621	0.621
30-40	0.114	0.448	0.0	0.621
40-50	0.128	0.576	0.172	0.793
50-70	0.132	0.708	0.106	0.899
70-90	0.115	0.823	0.0321	0.931
90-120	0.103	0.926	0.069	1.000
120-160	0.056	0.982	0.0	1.000
160-215	0.018	1.000	0.0	1.000

Table 4.4 : Different frequency distributions for the determination of spatial grain size distribution for 3 hours annealed sample.

Size class interval (μm)	Relative frequencies of linear itntercepts	Cumulative frequencies of linear intercepts	Normalised frequencies (normalised after –ve values were put to zero)	Cumulative frequencies of 3D grain diameter
0.0-25	0.374	.374	0.635	0.635
25-35	0.103	0.477	0.0	0.635
35-45	0.091	0.568	0.123	0.758
45-60	0.130	0.698	0.142	0.900
60-80	0.114	0.812	0.015	0.915
80-105	0.115	0.927	0.086	1.000
105-140	0.049	0.976	0.0	1.000
140-185	0.024	1.000	0.0	1.000

Table 4.5 : Different frequency distributions for the determination of spatial grain size distribution for 10 hours annealed sample

Size class interval (μm)	Relative frequencies of linear intercepts	Cumulative frequencies of linear intercepts	Normalised frequencies of 3D grain diameter (normalised after −ve values were put to zero)	Cumulative frequencies of 3D grain diameter
0.0-30	0.317	0.317	0.577	0.577
30-40	0.099	0.416	0.0	0.577
40-55	0.146	0.562	0.037	0.614
55-75	0.157	0.719	0.263	0.877
75-95	0.098	0.817	0.0	0.877
95-130	0.102	0.919	0.096	0.973
130-175	0.070	0.989	0.028	1.000
175-230	0.02	1.000	0.0	1.000

Table 4.6 : Different frequency distributions for the determination of spatial grain size distribution for 20 hours annealed sample

Size class interval (μm)	Realtive frequencies of linear intercepts	Cumulative frequencies of linear intercepts	Normalised frequencies (normalised after −ve values were put to zero)	Cumulative frequencies of 3D grain diameter
0.0-36	0.376	0.376	0.746	0.746
36-50	0.169	0.545	0.0	0.746
50-65	0.097	0.642	0.047	0.793
65-85	0.126	0.768	0.169	0.962
85-120	0.118	0.886	0.038	1.000
120-155	0.072	0.958	0.0	1.000
155-210	0.025	0.983	0.0	1.000
210-280	0.017	1.000	0.0	1.000

Table 4.7 : Different frequency distributions for the determination of spatial grain size distribution for 50 hours annealed sample

Size class interval (μm)	Relative frequencies of linear intercepts	Cumulative frequencies of linear intercepts	Normalised frequencies (normalised after -ve values were put to zero)	Cumulative frequencies of 3D grain diameter
0.0-45	0.516	0.516	0.841	0.841
45-65	0.189	0.705	0.0	0.841
65-85	0.149	0.854	0.136	0.977
85-110	0.073	0.927	0.0	0.977
110-145	0.039	0.966	0.0	0.977
145-195	0.025	0.991	0.018	0.999
195-265	0.006	0.997	0.005	1.000
265-350	0.003	1.000	0.0	1.000
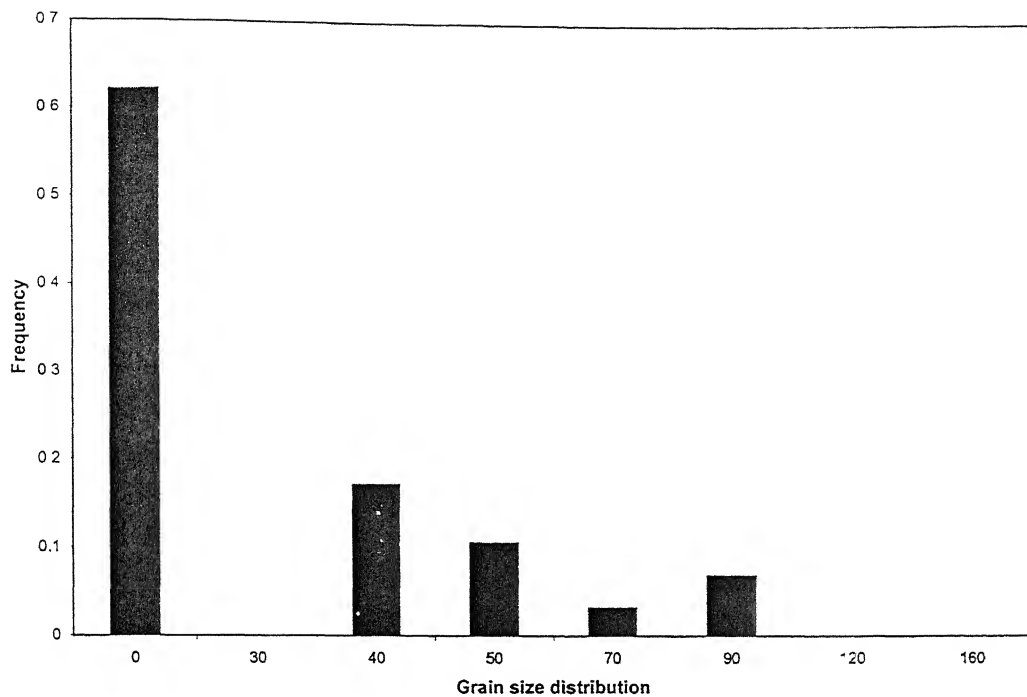
Figure 4.8 : Spatial grain size distribution of 1hour annealed sample.
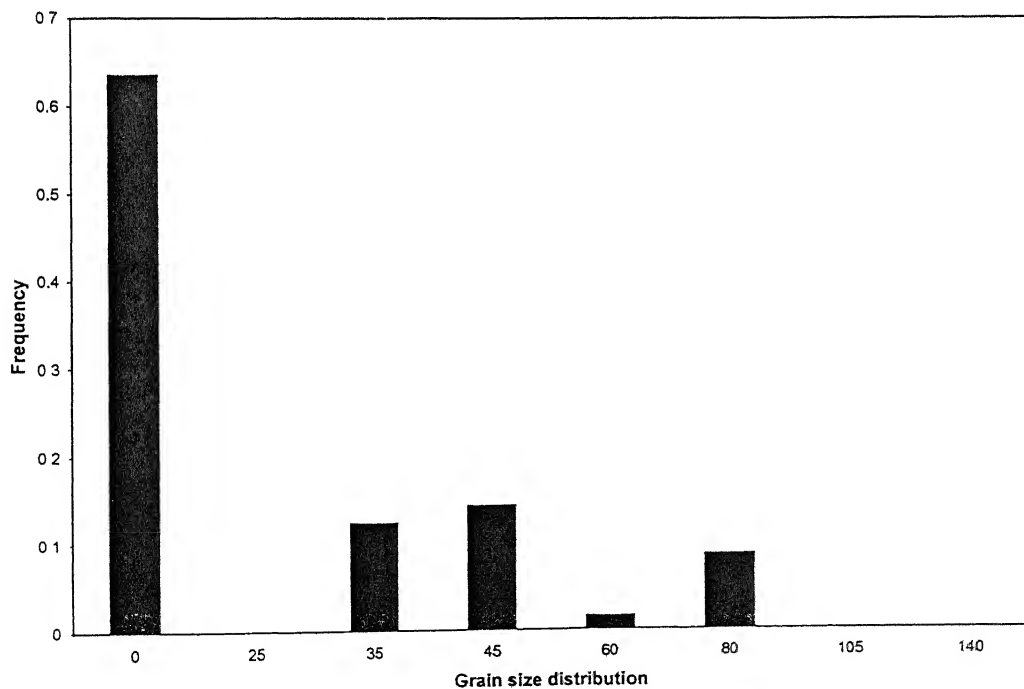
Figure 4.9 : Spatial grain size distribution of 3 hours annealed sample.
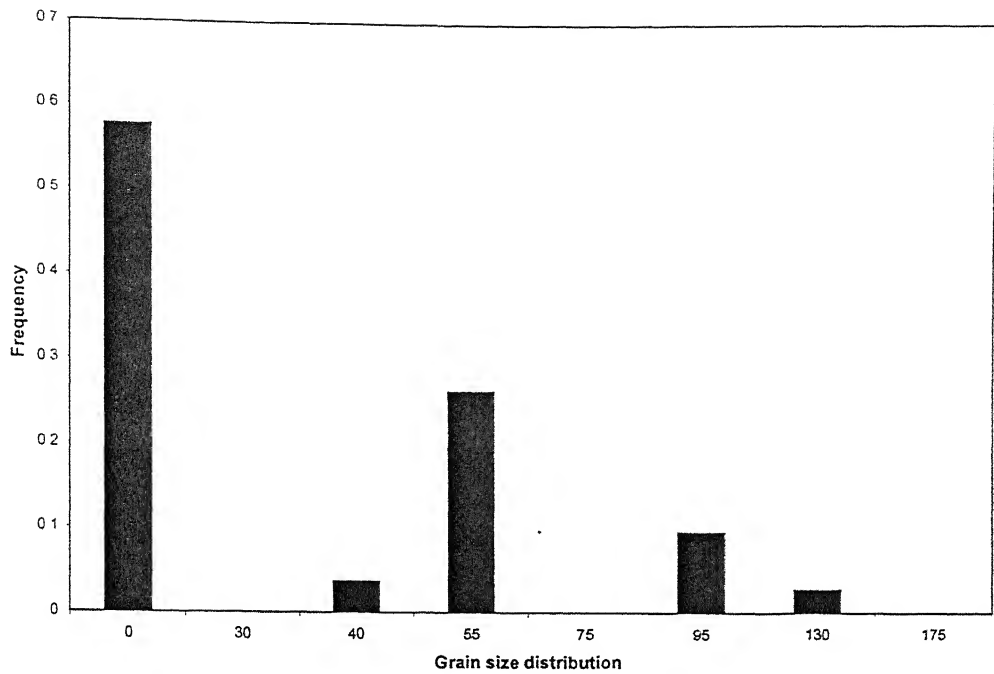
Figure 4.10 : Spatial grain size distribution of 10 hours annealed sample
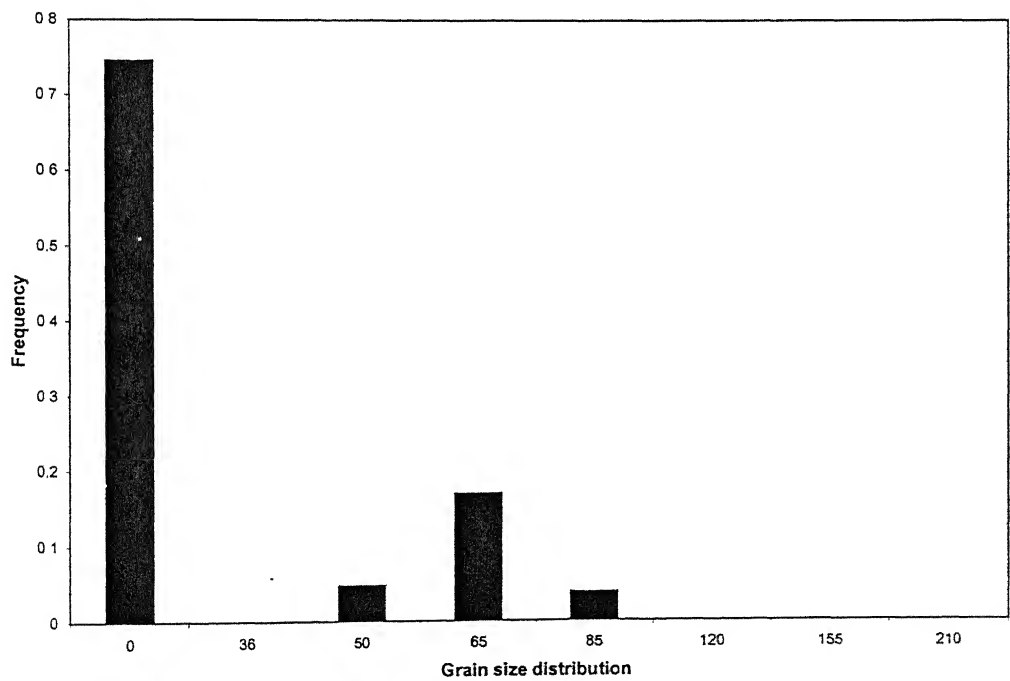
Figure 4.11 : Spatial grain size distribution of 20 hours annealed sample
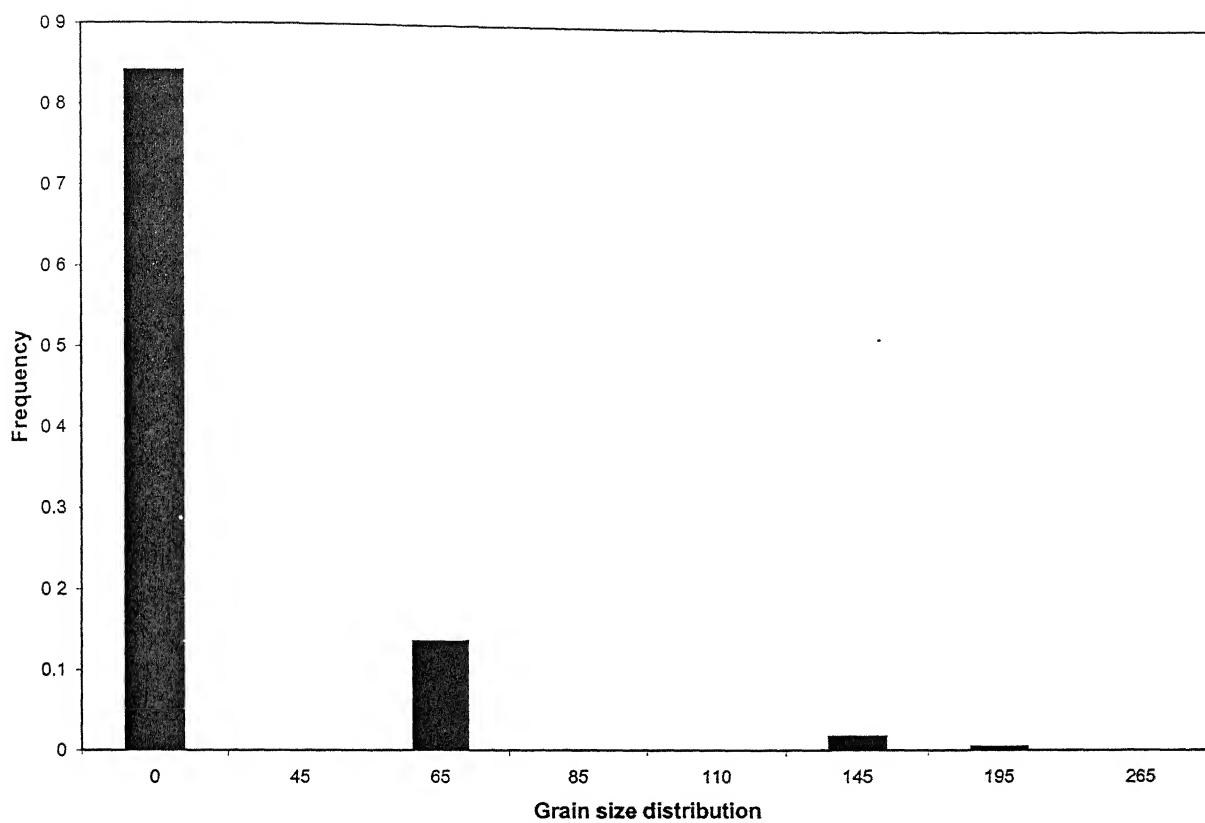
Figure 4.12 : Spatial grain size distribution of 50 hours annealed sample

4.1.2 Dihedral Angles

Plots of standard deviation of Plane dihedral angles distribution and the relative frequencies of $120°$ class $(110°-120°)$, are shown in figure 4.13 and 4.14 respectively. The relative frequencies of $110°$ class $(100°-110°)$ and $130°$ class $(120°-130°)$ of PDA distribution have been shown in table 4.8. The relative frequencies of $120°$ class (β_{120}) remains more or less constant with annealing time. The relative frequencies of PDA distribution of different annraled samples, at $800°$C are shown in figure 4.13. The various parameters of PDA distribution for all annealing treatments are also listed in table 4.8. The relative grain boundary energy distribution in polycrystals is an important microstructural parameter and has been analysed in this work. The entire analysis has been discussed in section 5.2

Table 4.8 : Calculated parameters of PDA distribution for annealing treatment at 800°C

Annealing time (hours)	Standard deviation of PDA distribution β_{SD}	Relative frequency of $110°$ class β_{110}	Relative frequency of $120°$ class β_{120}	Relative frequency of $130°$ class β_{130}
1	25.10	0.089	0.178	0.172
3	24.94	0.138	0.181	0.181
10	23.11	0.151	0.203	0.159
20	20.79	0.150	0.203	0.228
50	22.91	0.127	0.183	0.173
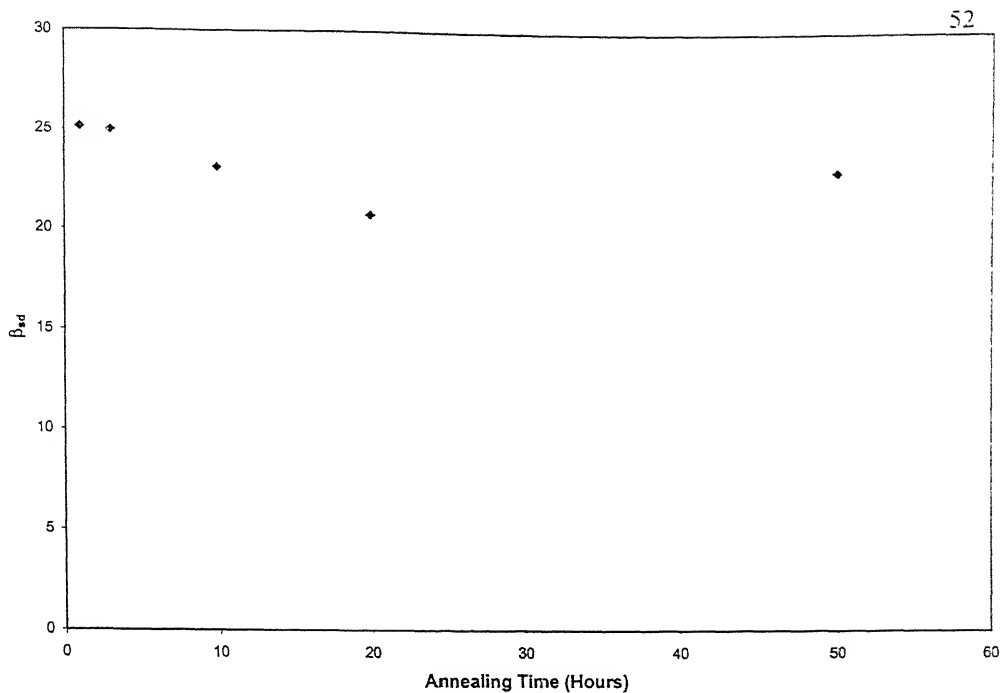
Figure 4.13 : Variation of standard deviation of PDA distributions with annealing time
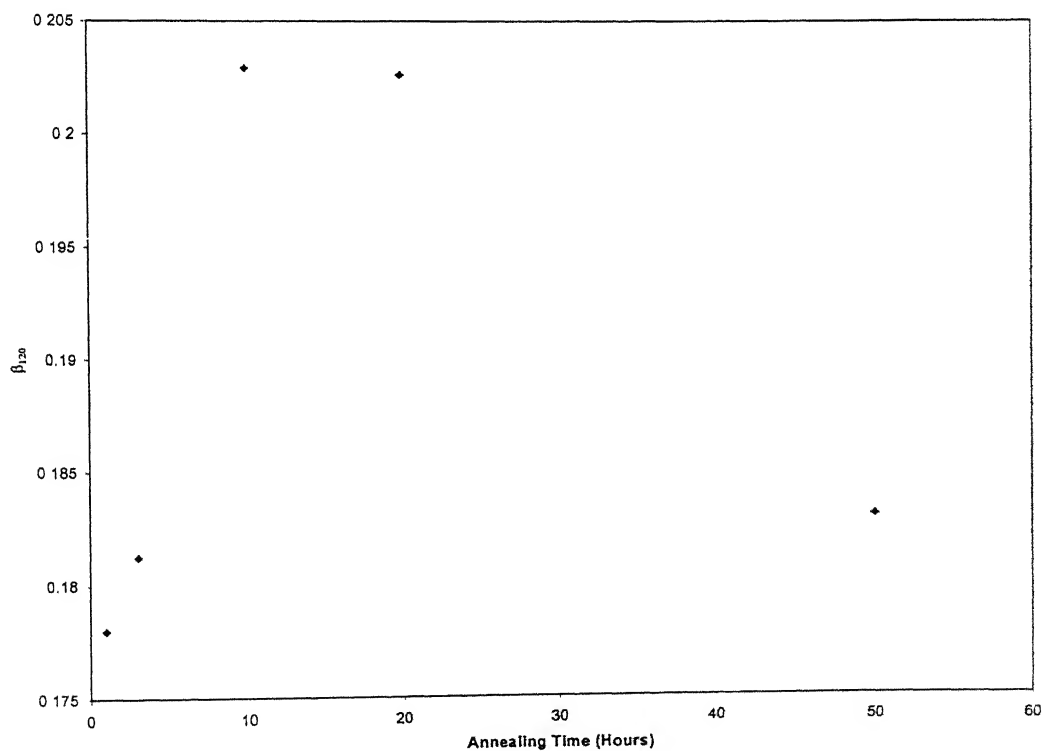
Figure 4.14 : Variation of Relative frequency of 110°-120° calss of PDA distributions with annealing time.
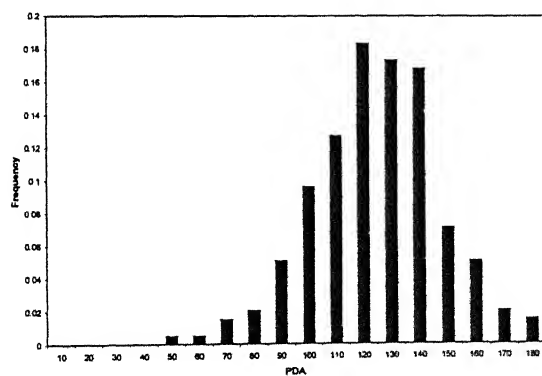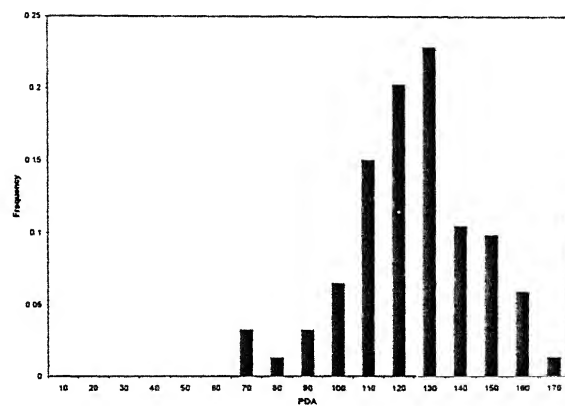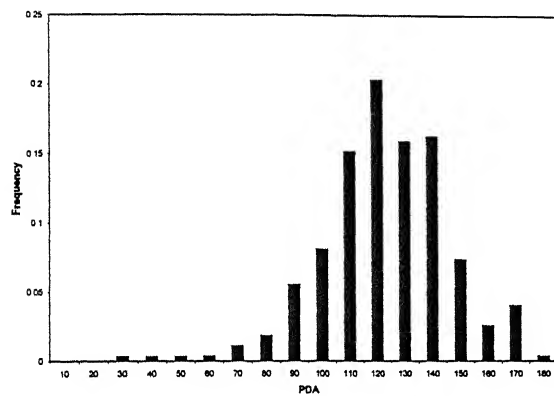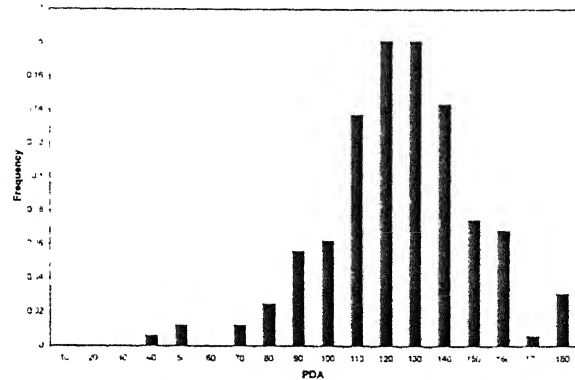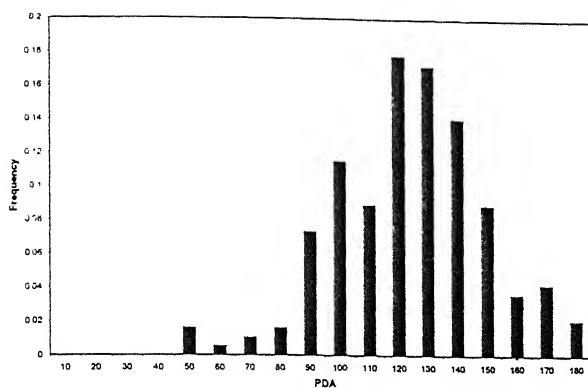
Fig 4.15 : Distribution of plane dihedral angles (PDA)of the annealed samples for
(a)1Hour, (b)3Hour,(c)10Hour,(d)20Hour,(e)50Hour at 800°

4.1.3 Fractal Dimensions

For fractal measurements, square grids of different sizes were placed over the microstructures and the number of squares N, that overlapped the grain boundaries were counted in each case. Plots of log(N) vs log(δ) for the five different annealed samples are presented in figures 4.17 to 4.21 and figure 4.16 shows the variation of fractal dimensions with annealing time. Table 4.9 presents the calculated fractal dimensions for different annealing treatments at 800°C.

Table 4.9 : Calculated Fractal Dimensions of different annealing treatments at 800°C.

Annealing Time in (hours)	1	3	10	20	50
Fractal Dimensions	0.991	0.9321	0.961	0.891	0.877
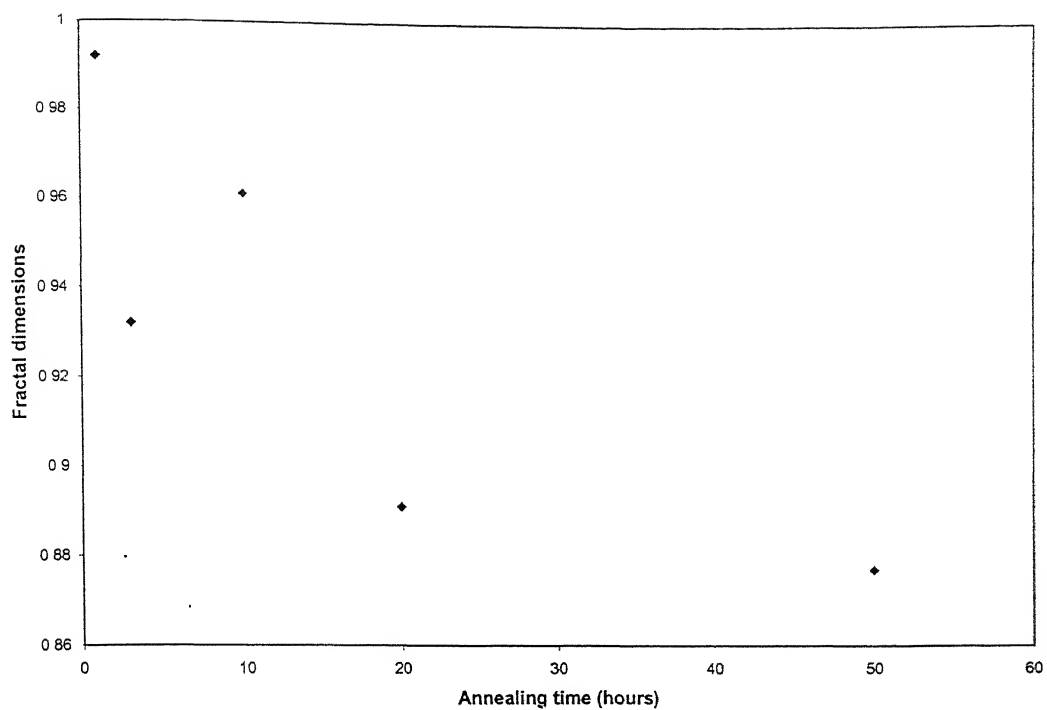
Figure 4.16 : Variation of fractal dimensions with annealing time.
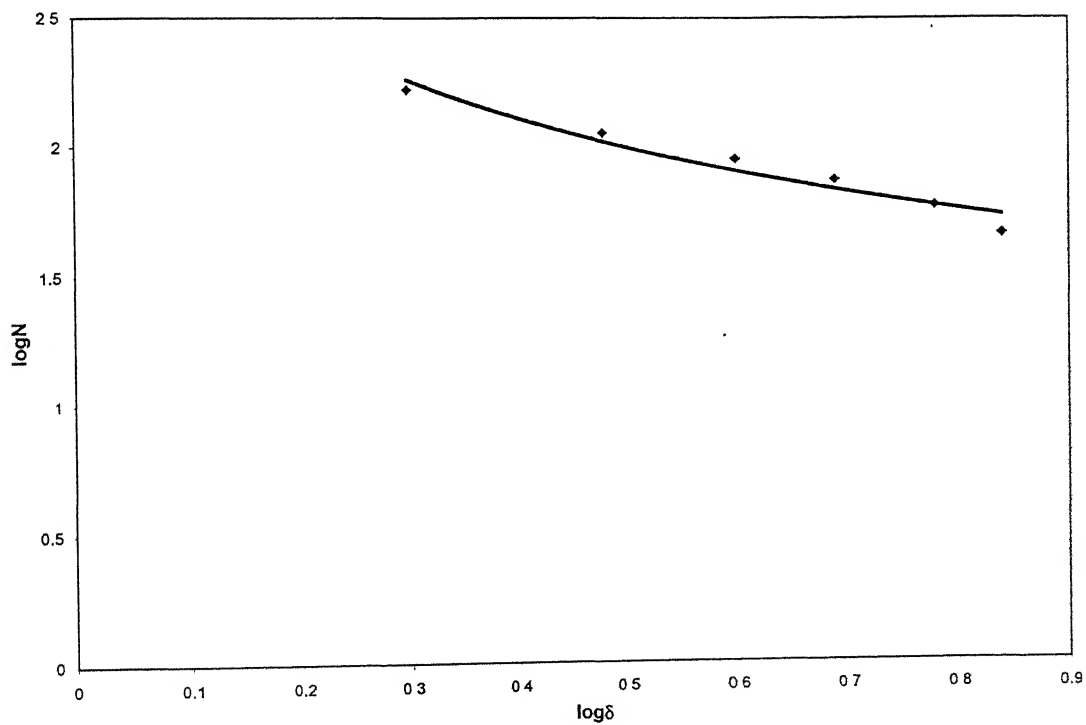
Figure 4.17 : logN vs logδ plot for 1 hour annealed sample.
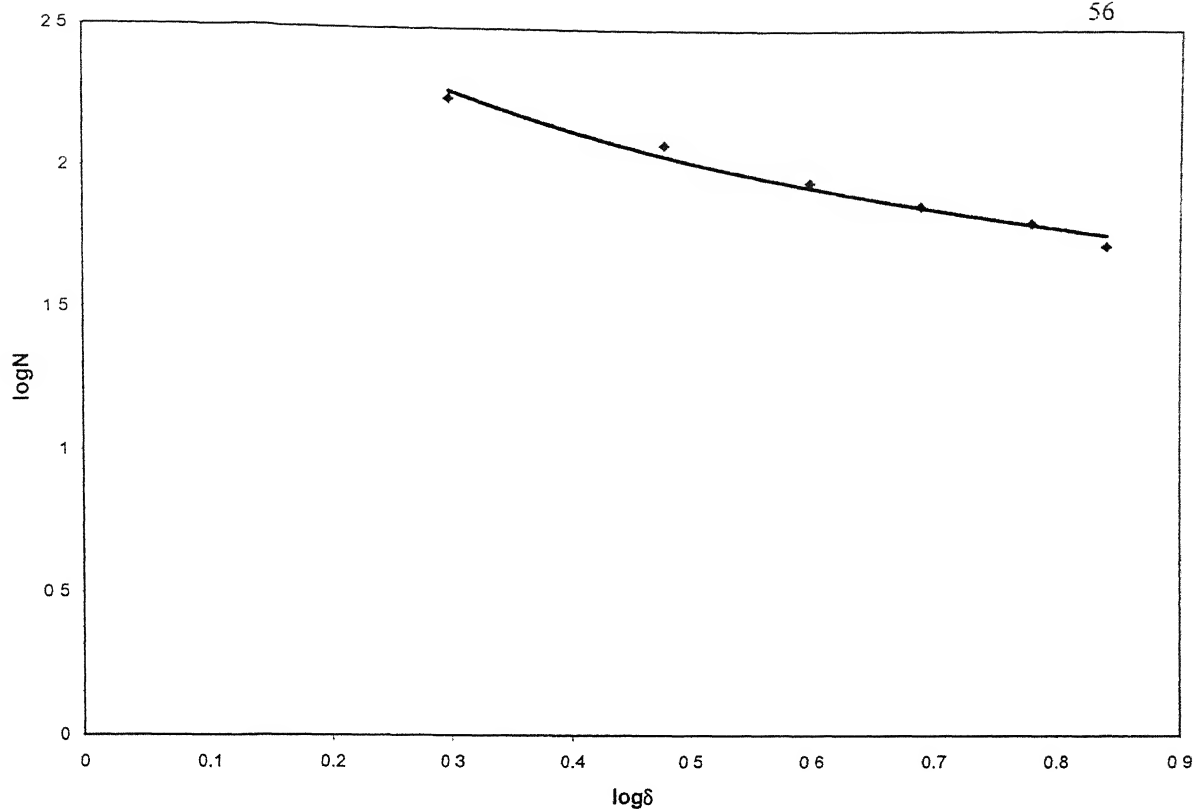
Figure 4.18 : Plot of logN vs logδ for 3 hours annealed sample.
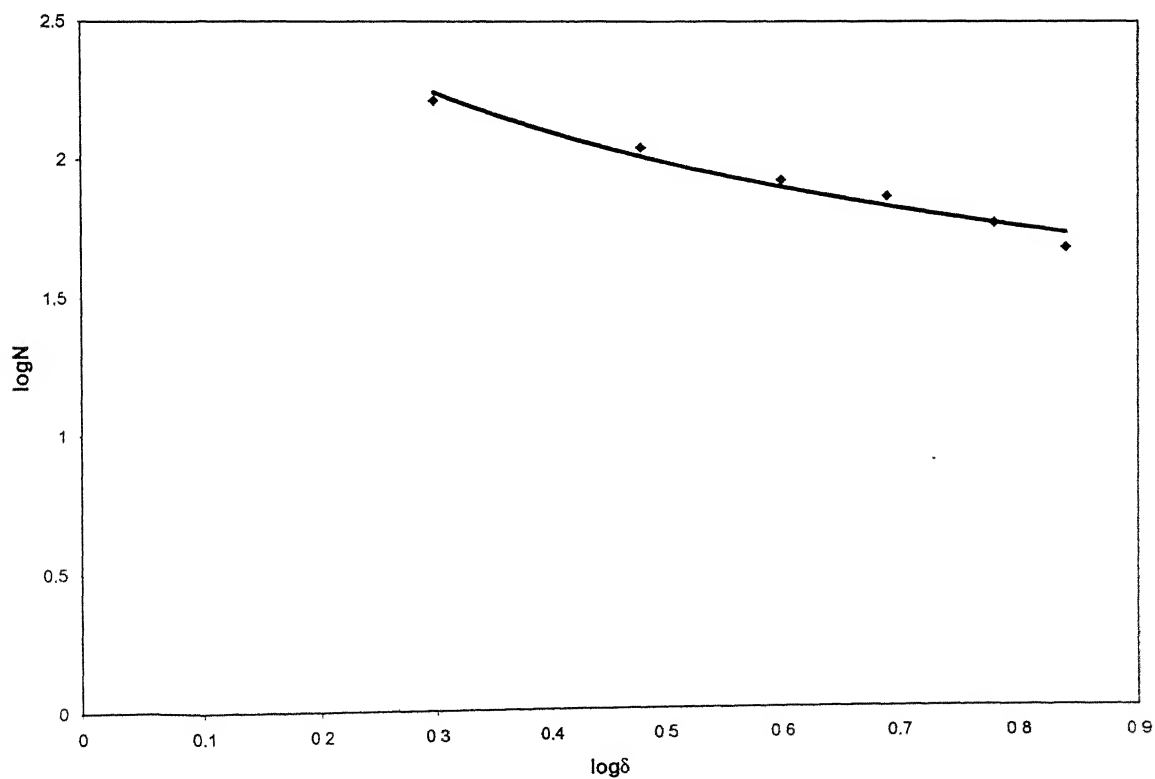
Figure 4.19 : Plot of logN vs logδ for 10 hours annealed sample.
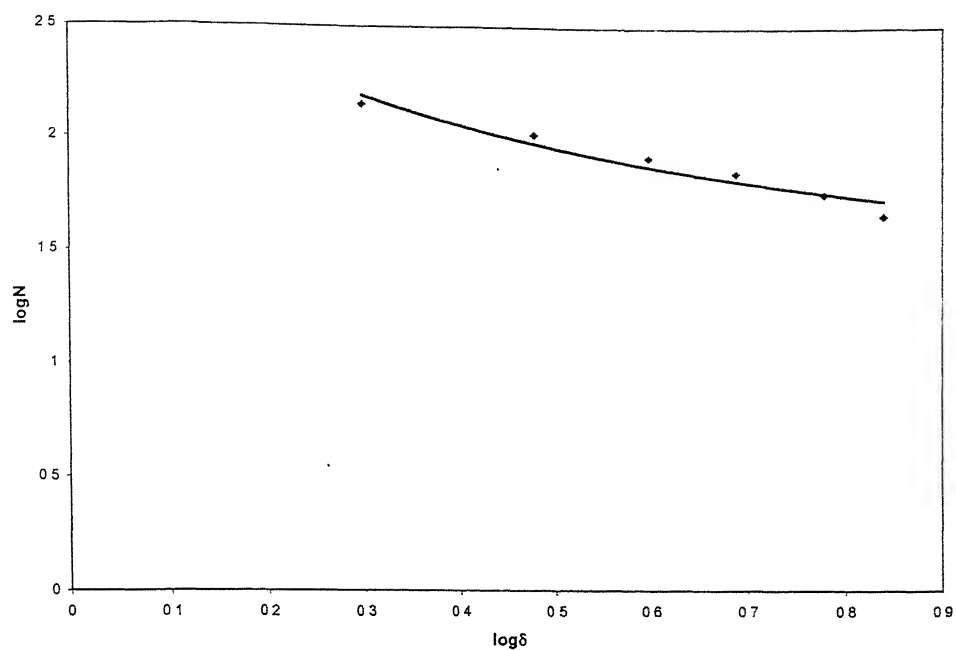
Figure 4.20 : logN vs logδ plot for 20 hours annealed sample.
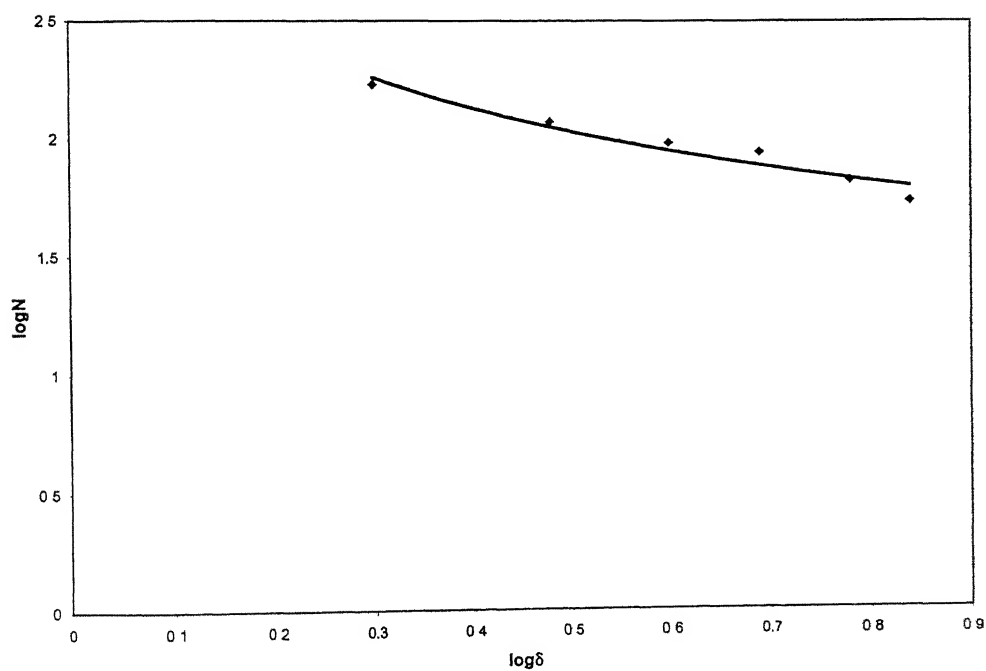
Figure 4.21 : logN vs logδ plot for 50 hours annealed sample.

4.2 Texture Result

Finally, Table 4.10, [19] gives the Volume Fractions and Intensity Values for {100}<001>Cube component, which are used in this attempt to find out the correlation of Microstructural Parameters with Texture.

Table 4.10 Texture Data for {100}<001>Cube Component

Annealing Time (hours)	f(g)	V% (considering random)		V% cube (without Random)
		% Random	V% cube	
1	23.2	42.8	23.8	41.6
3	32.6	39.6	27.6	45.7
10	27.8	41.2	25.2	42.8
20	34.6	25.2	33.5	44.7
50	32.7	40.8	27.8	46.9
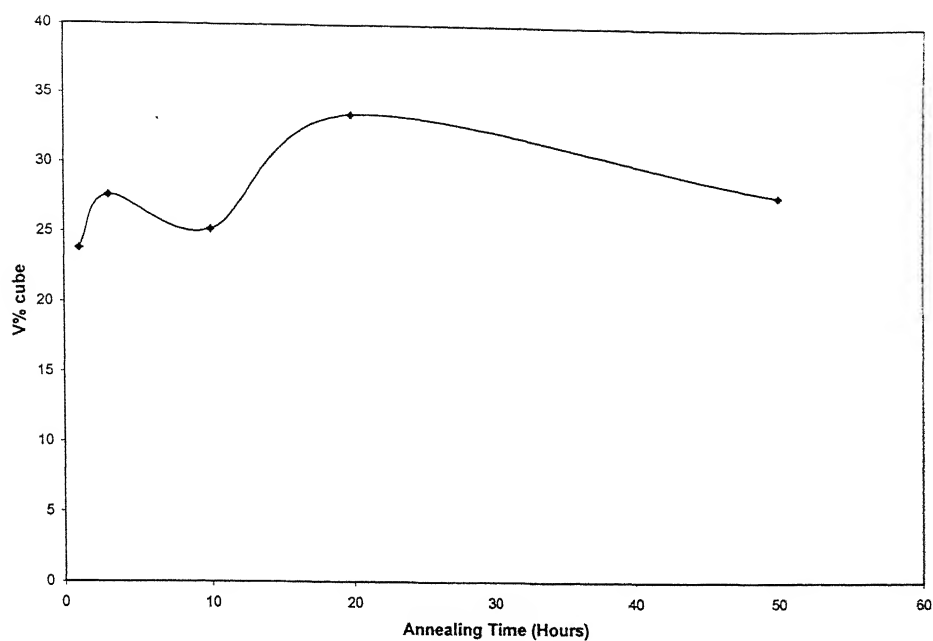
Figure 4.22 : Volume fraction of cube {100}<001> componenet considering random components
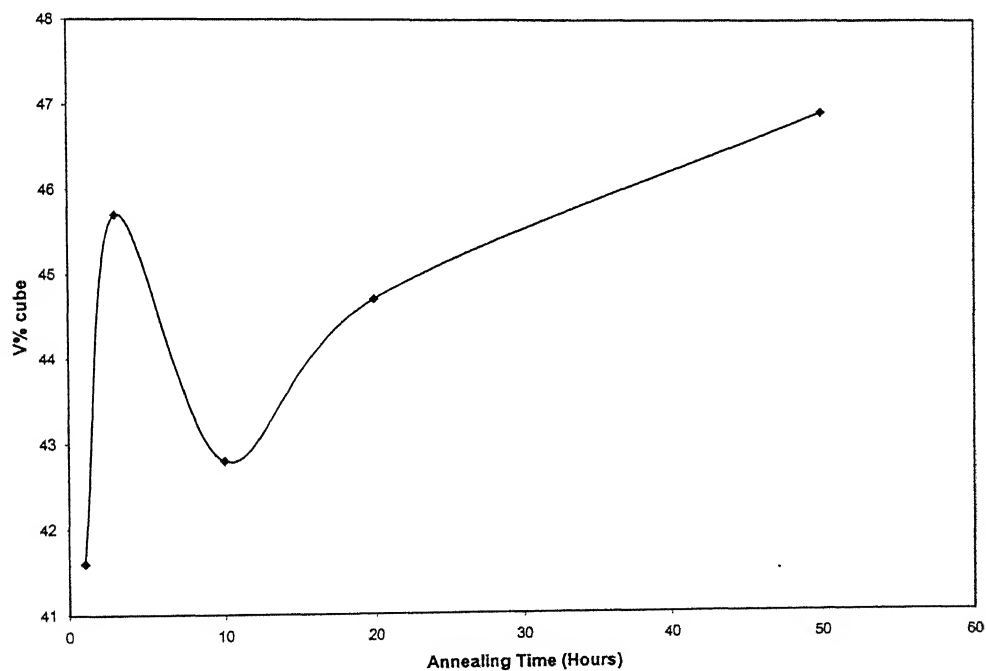
Figure 4.23 : Variation of volume fraction of cube {100}<001> component without consideration of random components.

Chapter 5

DISCUSSION

In the previous chapter, the experimental and calculated results of annealing treatment of five different samples at 800°C, for five different annealing time were presented. As already mentioned 95%cold rolled Ni-10%Co alloy was used for the study.The Microstructural parameters used for characterization of microstructures include analysis of grain size distribution, distribution of true dihedral angles (TDA) & grain boundary energy ratios and fractal dimensions.This chapter is divided into two sections.The first section analyses the variation of microstructural parameters with annealing treatment and the second section deals with the correlation of these microstructural parameters with the texture data of dominating cube {100}<001> componenet in the annealed samples.

5.1 Variation of Microstructural Parameters with Annealing Treatment

5.1.1 Grain Size

A spatial grain size distribution has been obtained using the matrix approach as discussed earlier. Table 4.3 to 4.7 of section 4.1.1 of previous chapter presents the work done for the determination of spatial grain size distribution for the five different annealed samples. Various parameters of mean intercept length with 95% confidence interval and standard deviation of intercept length distribution have been shown in table 4.1.It can be seen from the table that there is a continuous increase in the mean grain size. From the analysis of standard deviation and 95% confidence interval the increase in the grain size is statistically significant.

For the purpose of comparing the size distribution of the grains in the annealed samples, the cumulative frequency distributions were normalised with respect to the mean grain size. Figure 5.1(a) and 5.1(b) shows the variation of cumulative
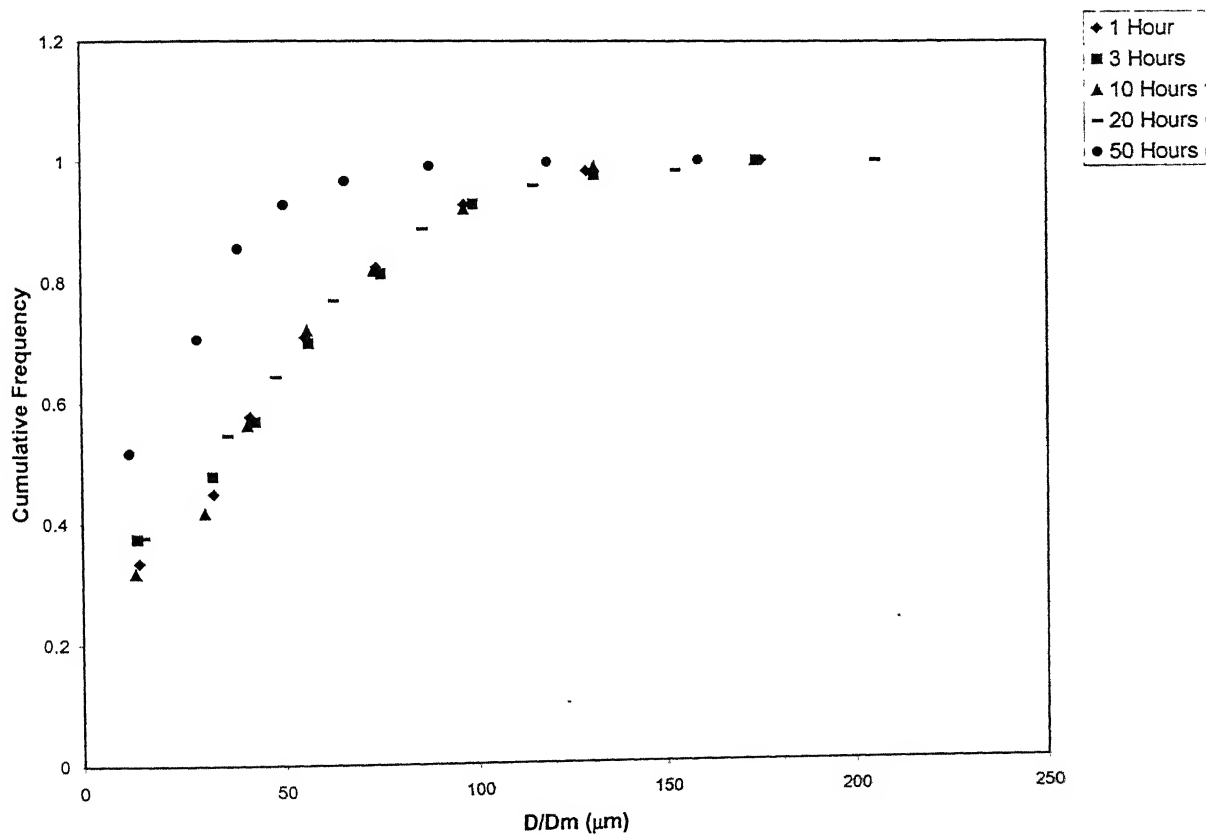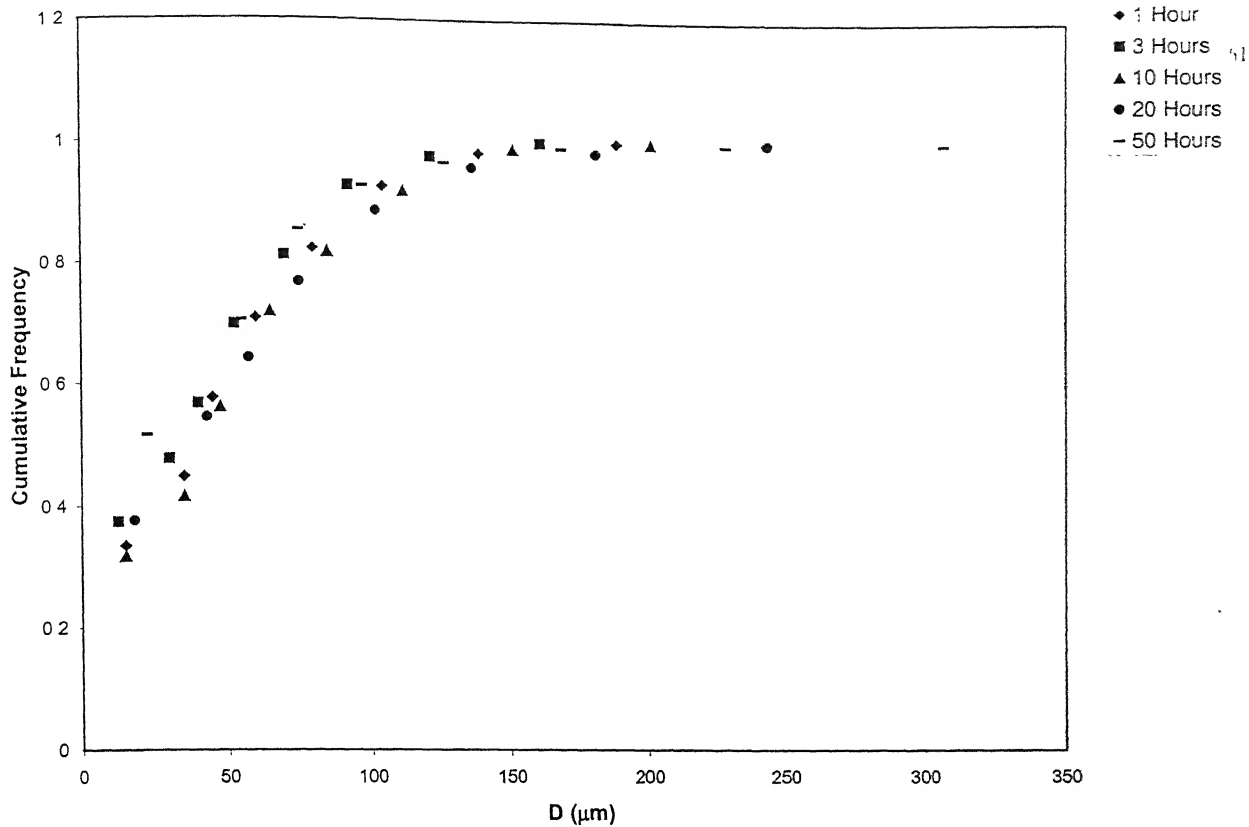
Figure 5.1 : (a) Cumulative frequency, and (b) Normalised cumulative frequency of intercept length distributions.

frequency of intercept length distribution and the normalised cumulative frequency of intercept length distribution respectively. and normalised grain diameter respectively. Following observations from normalised cumulative frequency curves of intercept length distributions can be made:

1 Upto the annealing time of 20 hours,the cumulative frequency curves completely overlap each other. This implies that the grain size distribution is similar in all the samples leading to the conclusion that the differences of the microstructures are related to each other by a scale factor.

2 However, in the case of the sample annealed at 50 hours, the normalisied distribution shows a distinctly different cumulative frequency curve as compared to the distributions obtained for other samples. Thus it is concluded that the grain size distribution of the 50 hours sample is significantly different from the other grain size distributions.

Intercept length distribution was transformed to spatial grain size distribution by using matrix equation given in section 2.1.1 of chapter 2. The 95% confidence interval cannot be determined for spatial distribution because the standard deviation of the sampling distribution cannot be calculated.

Figures 5.2(a) and 5.2(b) shows the variation of cumulative frequency and normalised for grain diameters (obtained from transformation). From these plots a scatter in the transformed distributions can be seen. On transformation it was observed that a few values of the relative frequencies of spatial grain size distribution are negative. In context of relative frequencies, the negative values have no physical significance. The method of transformation used is statistical in nature, and therefore relative frequencies will have certain statistical errors. It is expected that the observed negative values should correspond to actual realtive frequencies close to zero. The intercept lengths were measured manually from micrograph which may lead to errors in the measurements and may contribute to the errors in the transformed distribution. In view of the above the negative
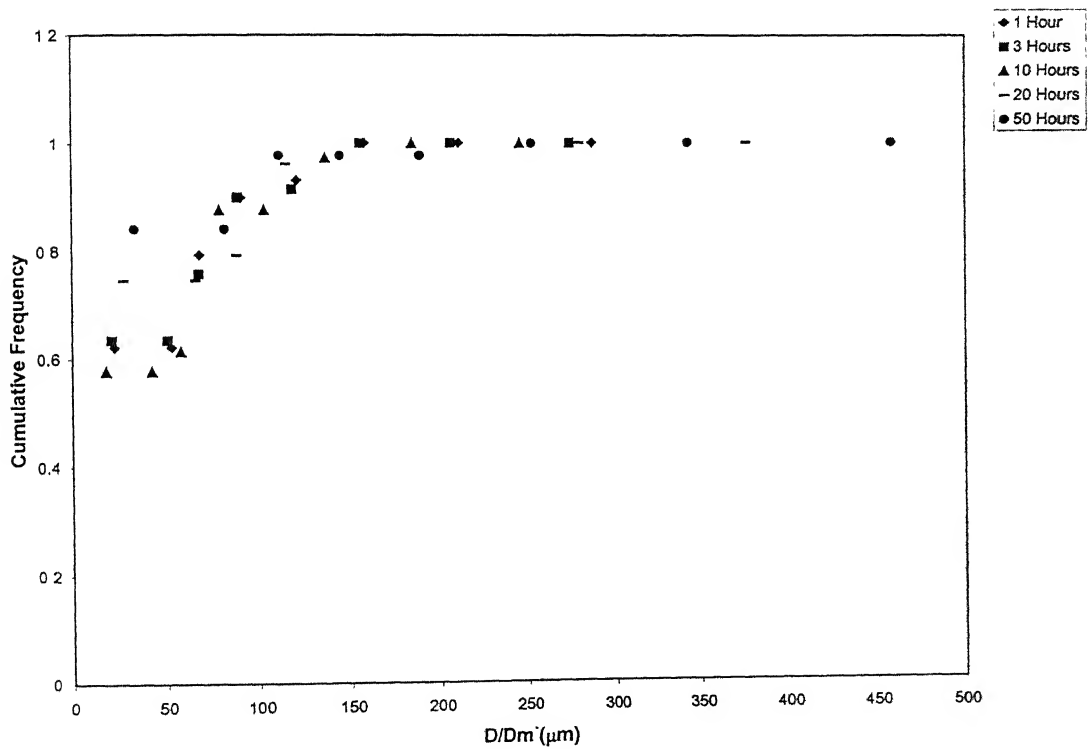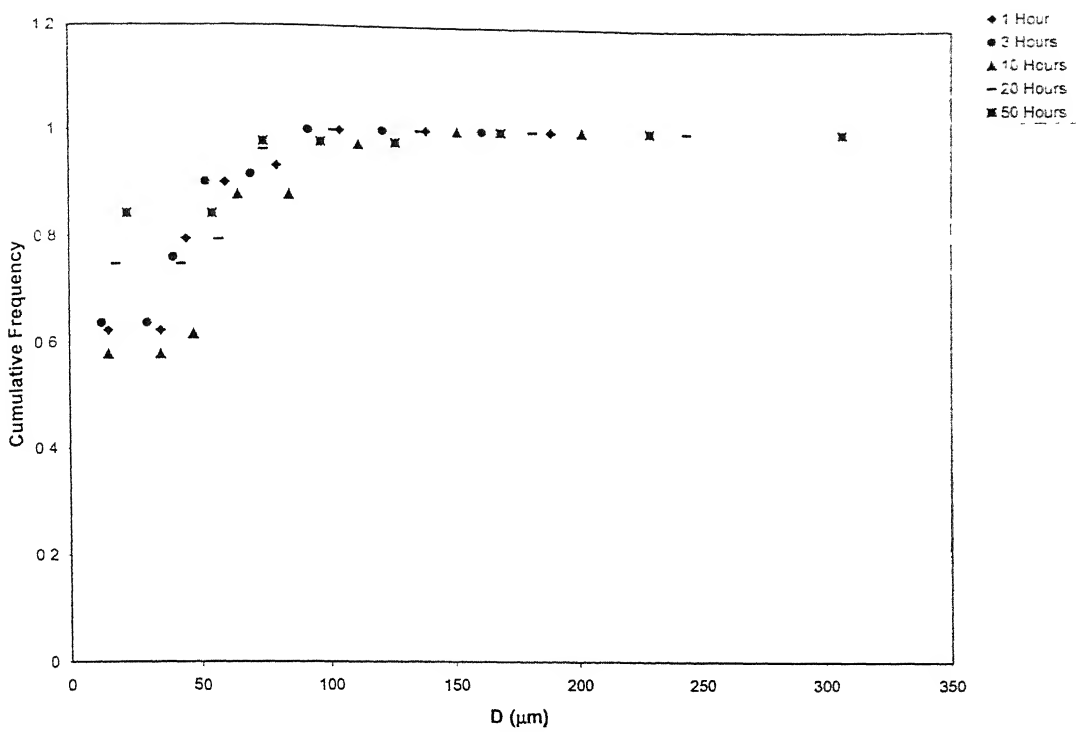
Figure 5.2 : (a) Cumulative ferquency, and (b) Normalisied cumulative frequency, distributions for grain diameter. (obtained from transformation).

relative frequencies were converted to zero and the frequencies were normalisied. This may have lead to the scatter observed in the spatial grain size distribution and hence no comparison could be done for the differently annealed samples. It is therefore suggested that using an optimisation technique with the constraint that all the relative frequencies must be greater than or equal to zero could be used to obtain spatial grain size distribution. Sach a technique may reduce the scatter in the transformed distribution.

5.1.2 Dihedral Angles

Different thermomechanical treatment can lead to grain boundaries with varying energy states. The variation in energy states results in differences in the distribution of plane dihedral angles. The relative frequency of 120°-130° class (β_{120}),and the standard deviation of PDA distribution (β_{SD}) remains more or less constant with annealing time (see figure 4.13). Based on the methodology presented in section 2.1.2.1, a programme was prepared for the transformation of plane dihedral angles to true dihedral angles. TDA distribution has been calculated from the measured plane dihedral angles using this programme. The computed values of the coefficient P_{ij} required for the transformatin of PDA to TDA are shown in table 5. The relative frequency of measured PDA and calculated TDA distribution for sample annealed for 1 Hour are presented in table 5.2. Table 5.1 below shows the various calculated parameters of TDA distribution

Table 5.1 Calculated Parameters for True Dihedral Angle Distribution for Sample Annealed at 800°C

Annealing time (hours)	Standard deviation of TDA distribution	Relative frequencies of 100°-120° class	Relative frequencies of 110°-120° class	Relative frequencies of 120°-130° Class
1	20.25	0.0	0.38	0.16
3	18.14	0.23	0.28	0.25
10	12.96	0.23	0.43	0.04
20	17.09	0.24	0.24	0.39
50	13.02	0.11	0.34	0.18

The distributions of PDAs have two components : (1) variation in the true dihedral angles at various triple edges, and (2) statistical variation due to the random orientations of the triple edges distributed in polycrystalline structure. The statistical variation (like random noise) tends to overshadow or hide the actual distribution of the true dihedral angles. The standard deviation of PDA distribution is effected by the above components. The latter contribution is eliminated during the process of transformation from PDAs to TDAs, the standard deviation deviation decreases and the peak height of the distribution increases significantly .Table 5.2 also clearly shows the reduction of the spread of the distribution on transformation from plane to true dihedral angles. The relative frequencies of TDA distribution for different annealed samples are shown in figure 5.5. The standard deviation of TDA distribution (α_{SD}) are calculated for different annealing treatments and are presented in figure 5.3. The relative frequencies of 110°-120° class of TDAs is also shown in figure 5.3
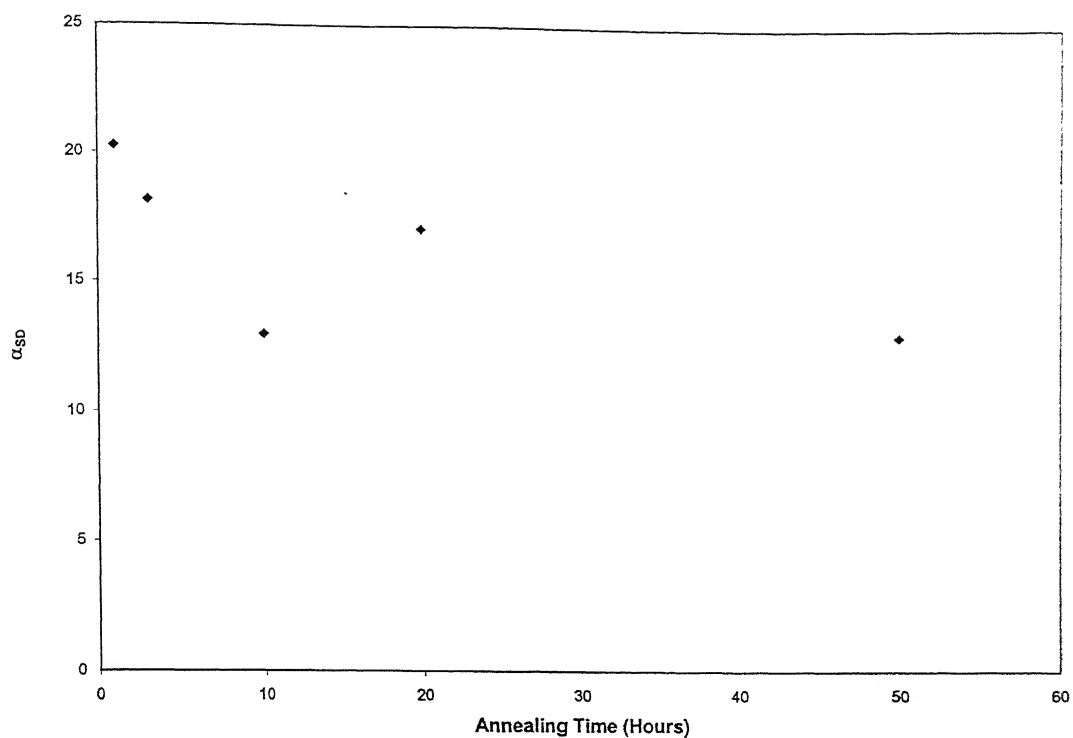
Figure 5.3 : Variation of standarad deviation ofTDA distributions with annealing time.
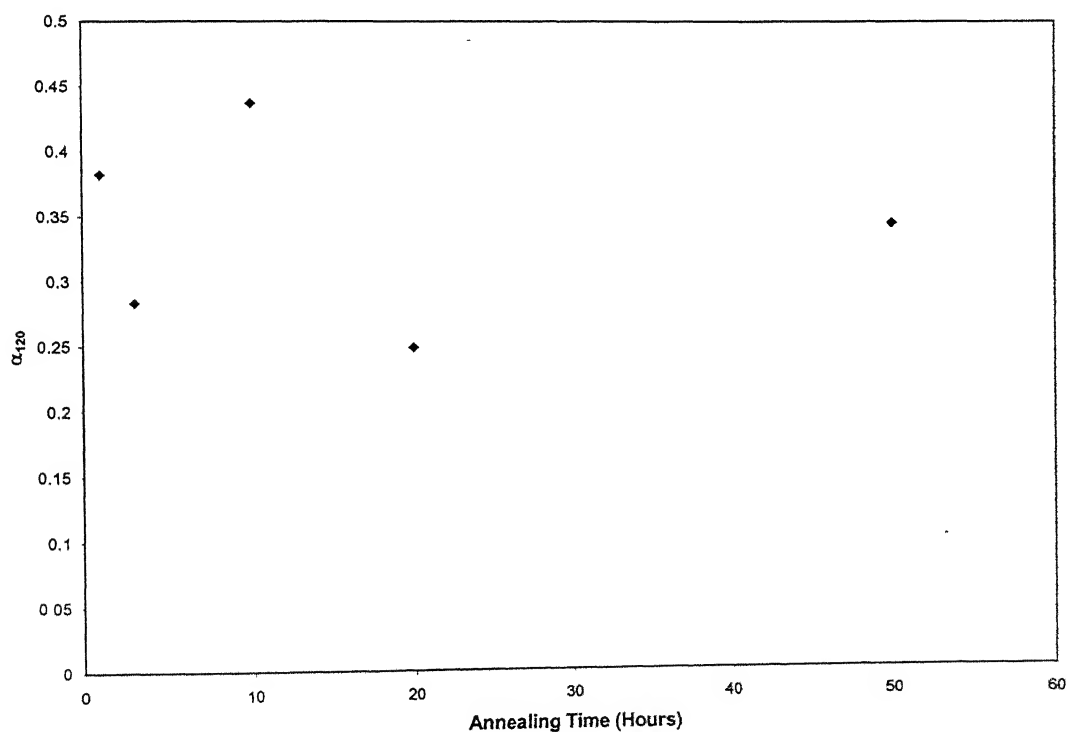
Figure 5.4 : Variation of relative frequency of 110°-120° class of TDA distributions with annealing time.
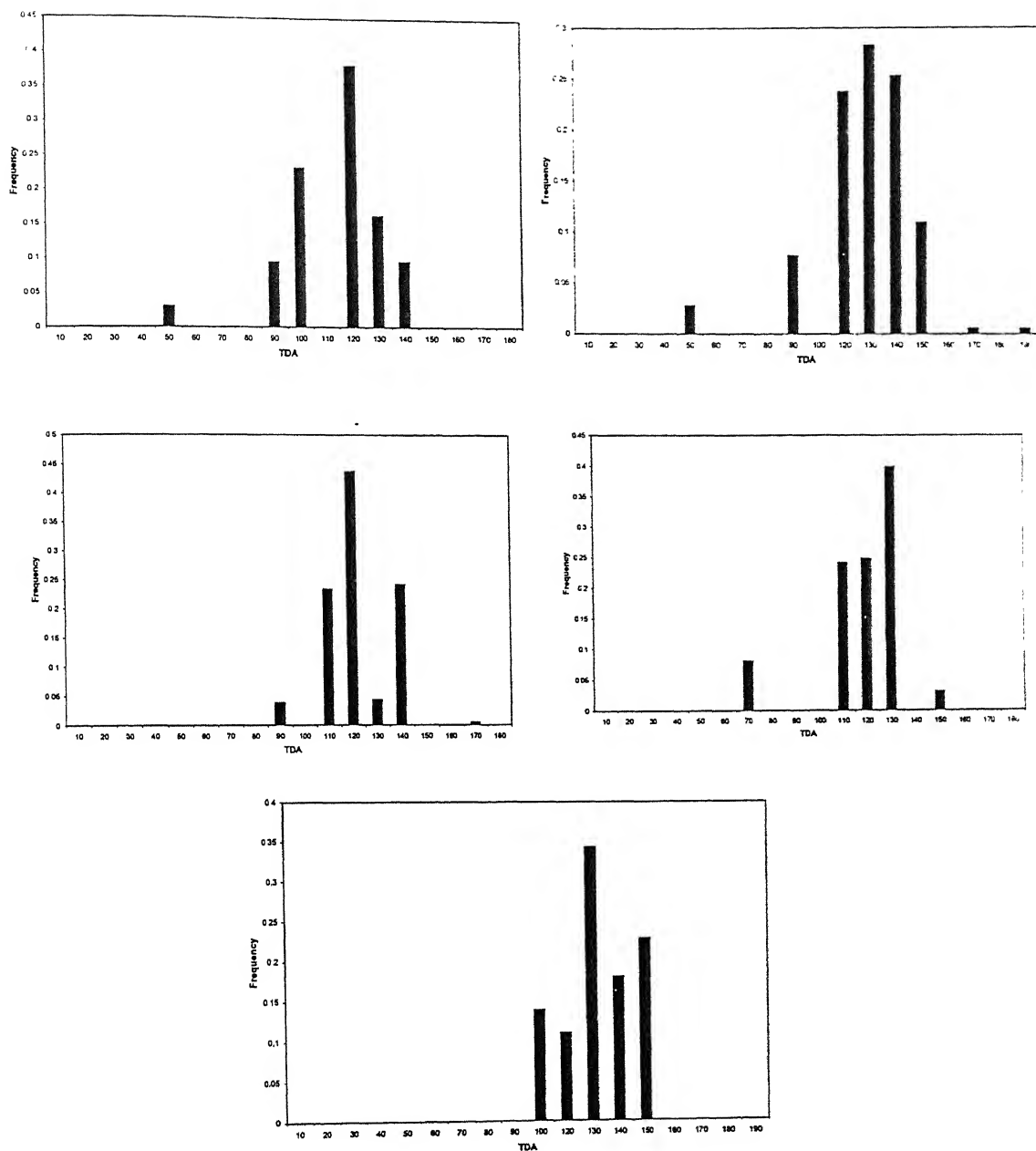
Fig 5.5 : Distribution of true dihedral angle(TDA) of the annealed sample annealed for (a)1Hour,(b)3Hours,(c)10Hours,(d)20Hours,(e)50Hours at 800°

Table 5.2 Relative frequencies of measured PDA distribution and calculated TDA distribution of sample annealed at 800°C and 1 hour

Class Range (Degrees)	Frequency of Plane Dihedral Angles (β)	Frequency of True Dihedral Angles (α)
0-10	0.0	0.0
10-20	0.0	0.0
20-30	0.0	0.0
30-40	0.0	0.0
40-50	0.016	0.03
50-60	0.005	0.0
60-70	0.010	0.0
70-80	0.016	0.0
80-90	0.073	0.095
90-100	0.115	0.233
100-110	0.089	0.0
110-120	0.178	0.382
120-130	0.172	0.163
130-140	0.140	0.096
140-150	0.089	0.0
150-160	0.036	0.0
160-170	0.042	0.0
170-180	0.020	0.0

It is known that, the relative grain boundary distribution in polycrysatals is an important microstructural parameter and has been analysed in this work. Equation 2.1 (given in section 2.1.2) which relates grain boundary energies to TDA is reproduced below.

$$\frac{\gamma_1}{\sin \alpha_1} = \frac{\gamma_2}{\sin \alpha_2} = \frac{\gamma_3}{\sin \alpha_3}$$

where,

γ_1, γ_2 and γ_3 are the energy per unit area of the grain boundary plane.

and,

α_1, α_2 and α_3 are the true dihedral angles.

As mentioned in previous chapter the convention adopted here is :

$\alpha_1 > \alpha_2 > \alpha_3$, which results in $\gamma_3 > \gamma_2 > \gamma_1$.

The energy ratios γ_3/γ_1 corresponding to the lowest and highest, and γ_2/γ_1 corresponding to the second highest and highest of the three TDAs were calculated and their distributions analysed as discussed below:

In order to calculate these ratios, the following procedur was adopted. At each of the triple points of the micrographs, PDAs β_1,β_2 and β_3 were measured, which correspond to α_1, α_2 and α_3. The distribution of the highest β (denoted as β_1) and smallest β (denoted as β_3) were obtained. From the distribution of β_1 and β_3 the corresponding distributions of α_1(highest) and α_3(lowest) were obtained using the method discussed in section 2.1.2.1. The joint distribution of α_1 and α_3 was obtained by the following relation:

$$p(\alpha_1, \alpha_3) = p_1(\alpha_1)\, p_2(\alpha_3)$$

Where $p(\alpha_1, \alpha_3)$ is the probability (frequency) that the angles at a triple edge will be in the range α_1 to $\alpha_1+\Delta\alpha_1$ and $\alpha_3+\Delta\alpha_3$

$p_1(\alpha_1)$ is the probability that the angle at a triple edge be in the range α_1 to $\alpha_1+\Delta\alpha_1$ for feasible value of α_3.

$p_2(\alpha_3)$ is the probability that the angle at a triple edge will be in the range α_3 to $\alpha_3+\Delta\alpha_3$ for feasible value of α_1.

This entire analysis has been presented in table, 5.3 to 5.7, for the five differently annealed samples.

Table 5.3 : Analysis of grain boundary energy distribution for 1 hour annealed sample

α_1 (degrees)	α_2 (degrees)	Probabilty of Occurrence Of α_1 and α_2	γ_3/γ_1	γ_2/γ_1
130	110	0.04	1.23	1.13
130	100	0.20	1.29	1.00
130	90	0.18	1.31	.83
140	110	0.07	1.46	1.46
160	100	0.07	2.88	2.87
160	90	0.03	2.92	2.74
170	90	0.02	5.76	5.76

Table 5.4 : Analysis of grain boundary energy distribution for 3 hours annealed sample

α_1	α_2	Probability of Occurrence Of α_1 and α_3.	γ_3/γ_1	γ_2/γ_1
130	110	0.42	1.23	1.13
140	110	0.46	1.46	1.46
150	90	0.02	2.00	1.73
150	70	0.01	1.88	1.28

Table 5.5 : Analysis of grain boundary energy distribution for 10 hours annealed sample

α_1	α_3	Probability of Occurrence Of α_1 and α_3	γ_3/γ_1	γ_2/γ_1
130	110	0.13	1.23	1.13
130	100	0.03	1.28	1.00
140	110	0.59	1.46	1.46
140	100	0.12	1.53	1.34
140	90	0.12	1.55	1.19
170	90	0.01	5.76	5.67

Table 5.6 : Analysis of grain boundary energy distribution for 20 hours annealed sample

α_1	α_3	Probability of Occurrence of α_1 and α_3	γ_3/γ_1	γ_2/γ_1
130	110	0.80	1.23	1.13
130	100	0.10	1.28	1.00
150	100	0.02	1.97	1.87
150	90	0.01	2.00	1.73
150	70	0.05	1.88	1.28
160	70	0.01	2.75	2.23

Table 5.7 : Analysis of grain boundary energy distribution for 50 hours annealed sample

α_1	α_3	Probability of Occurrence of α_1 and α_3	γ_3/γ_1	γ_2/γ_1
130	110	0.15	1.23	1.13
130	100	0.24	1.28	1.00
130	90	0.13	1.30	0.83
140	110	0.18	1.46	1.46
140	100	0.29	1.53	1.34
160	100	0.01	2.87	2.87

The distribution for γ_3/γ_1 and γ_2/γ_1 are shown in table.5.2 and 5.3 and graphically these distributions are shown in from figures.5.1 to 5.7 respectively.

Table 5.8 Distribution of γ_3/γ_1 for different annealing time.

Energy class interval	Annealing Time (Hours)				
	1 Hour Frequency	3 Hours Frequency	10 Hours Frequency	20 Hours Frequency	50 Hours Frequency
1.0-1.5	0.31	0.88	0.87	0.90	0.99
1.5-2.0	0.57	0.03	0.12	0.08	0.0
2.0-2.5	0.0	0.0	0.0	0.0	0.0
2.5-3.0	0.1	0.0	0.0	0.01	0.01
3.0-3.5	0.0	0.0	0.0	0.0	0.0
3.5-4.0	0.0	0.0	0.0	0.0	0.0
4.0-4.5	0.0	0.0	0.0	0.0	0.0
4.5-5.0	0.0	0.0	0.0	0.0	0.0
5.0-5.5	0.0	0.0	0.0	0.0	0.0
5.5-6.0	0.02	0.0	0.01	0.0	0.0

Table 5.9 : Distribution of γ_2/γ_1 for different annealing time

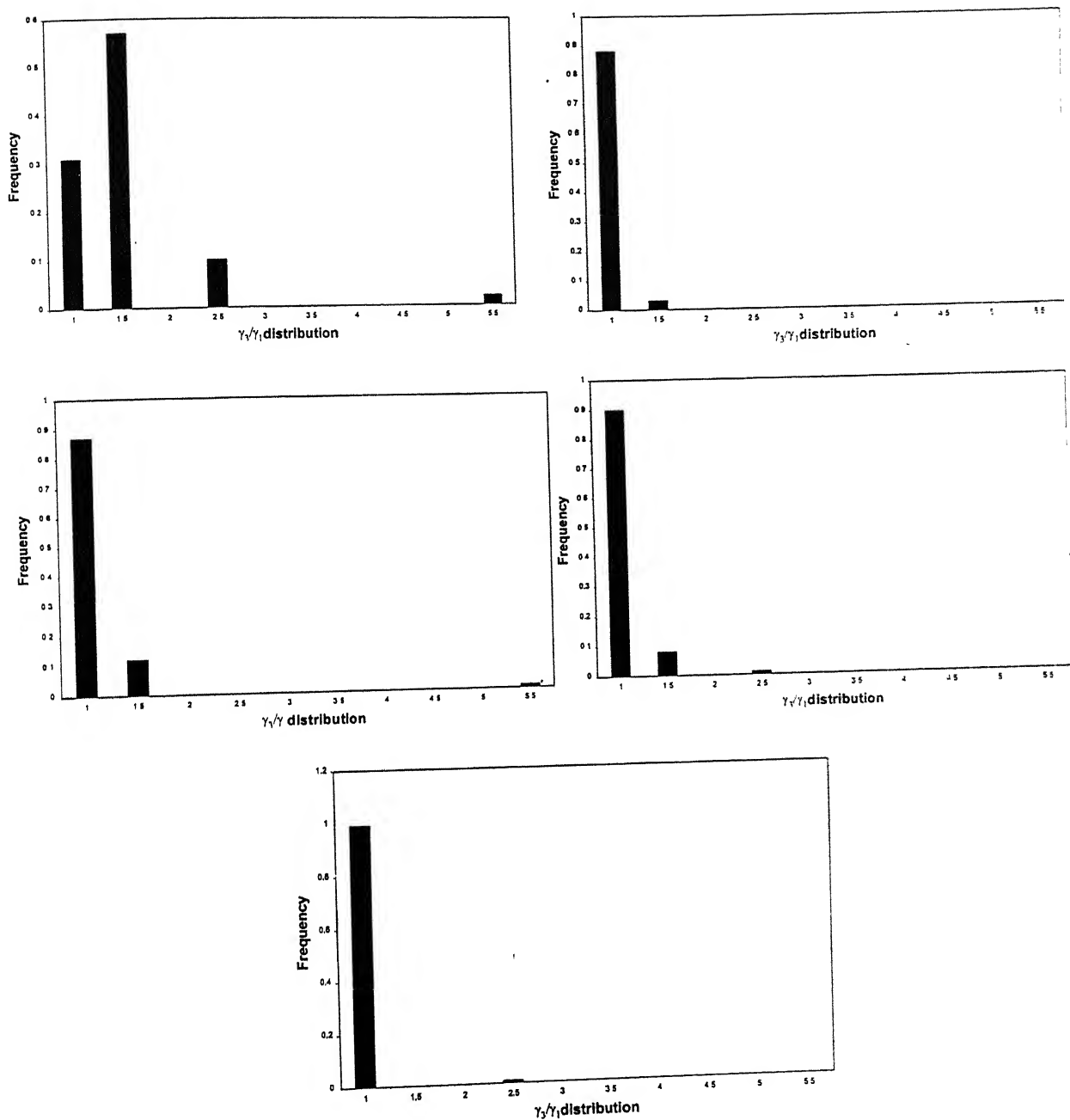| Energy class interval	Annealing Time (Hours)				
	1 Hour Frequency	3 Hours Frequency	10 Hours Frequency	20 Hours Frequency	50 Hours Frequency
1.0-1.5	0.88	0.89	0.99	0.95	0.99
1.5-2.0	0.0	0.02	0.0	0.03	0.0
2.0-2.5	0.0	0.0	0.0	0.01	0.0
2.5-3.0	0.1	0.0	0.0	0.0	0.01
3.0-3.5	0.0	0.0	0.0	0.0	0.0
3.5-4.0	0.0	0.0	0.0	0.0	0.0
4.0-4.5	0.0	0.0	0.0	0.0	0.0
4.5-5.0	0.0	0.0	0.0	0.0	0.0
5.0-5.5	0.0	0.0	0.0	0.0	0.0
5.5-6.0	0.02	0.0	0.01	0.0	0.0

Figure 5.6 : Distribution of γ_3/γ_1 energy ratios of the annealed samples annealed for (a) 1 hour, (b) 3 hours, (c) 10 hours, (d) 20 hours, (e) 50 hours.
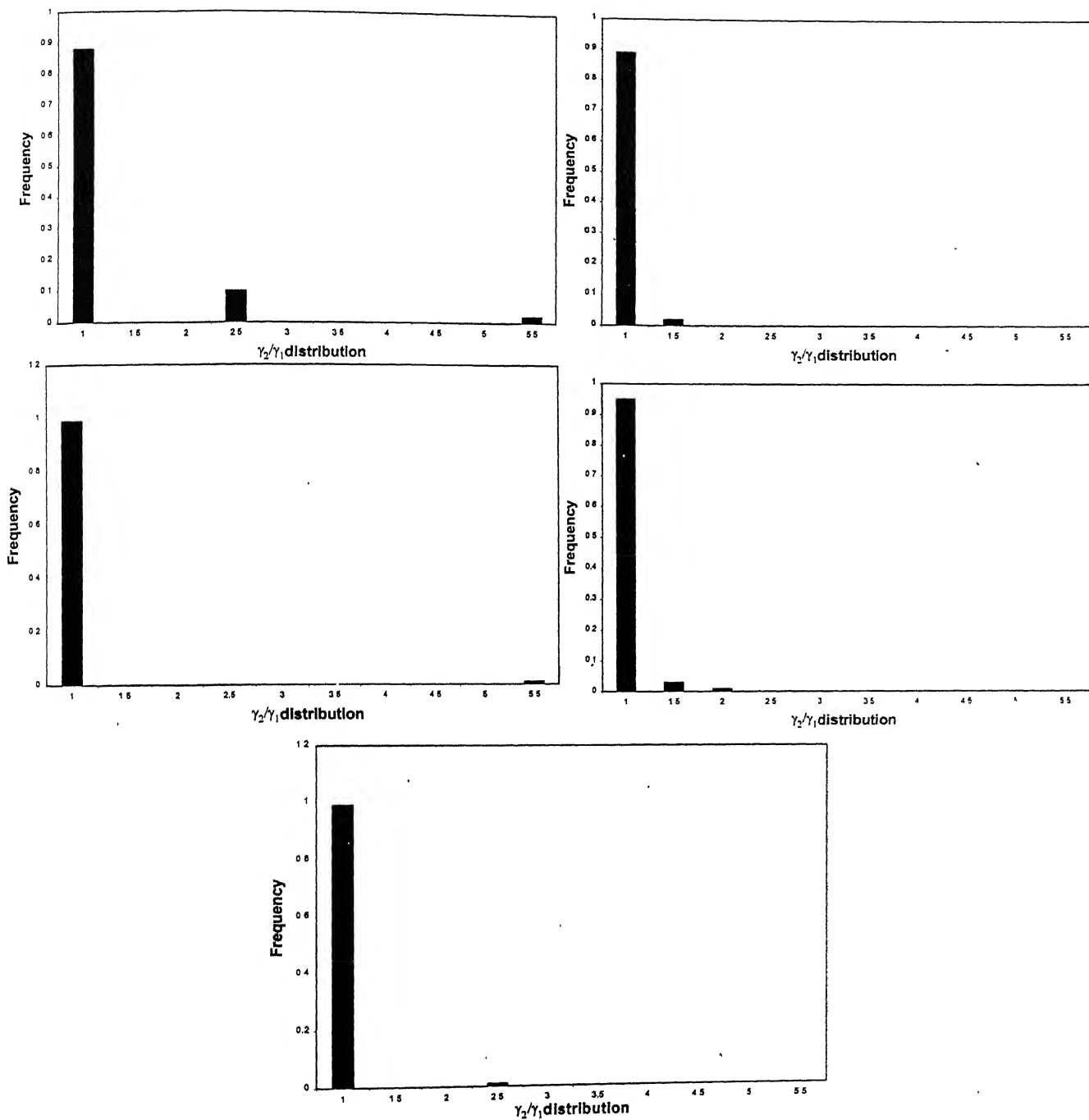
Figure 5.7 : Distribution of γ_2/γ_1 energy ratios of the annealed samples ,annealed for (a) 1 hour, (b) 3 hours, (c) 10 hours, (d) 20 hours, (e) 50 hours.

Figures 5.6 and 5.7 show γ_3/γ_1 and γ_2/γ_1 distribution at different annealing time. It is cleared from the figures that the energy ratio tend towards unity as annealing time increases. Significance of the analysis energy ratios is discussed in section 5.2.

5.1.3 Fractal Dimension

The concept of fractal geometry serves as an efficient tool to characterize the rugged grain boundaries . For rugged profiles the value of fractal dimension D lie between 1 and 2. Rugged grain boundaries correspond to a certain value of fractal dimension. Table 4.9 of section 4.1.3 presents the fractal dimension of the five different annealed sample. In each of the sample, the fractal dimension is close to 1, which suggests that the grain boundaries are not rugged. The fractal dimension should not be less than unity for lines. The slight decrepancy from 1 may be due to the broken lines resulting from incomplete etching not accounted for during measurements in the sample.

5.2 Correlation of microstructural parameters with texture

The texture data for the most dominanat cube {100}<001> component ,as a function of annealing time at 800° C, have been displayed in table 4.10 of section 4.2 . It is clear from the table, that although there are minor variations in the volume fractions of the cube componenet at different stages of annealing,by and large, these variations are not that significant . In fact ,the volume fractions of the cube componenet is found to maintain almost similar values as annealing progress, with the exception of the 20 Hours annealed sample

The entire grain boundary energy analyses discussed in the previous section also shows this. The distributions of two grain boundaries ratios of γ_3/γ_1 and γ_2/γ_1 are tending to 1 with annealing. This indicates that the boundaries are not much different from one another energywise..Thus whatever boundary movement takes place during the grain growth process is not likely to be dependent on the individual grain boundary energies. In fact it appears that there is a continuous

urge among the boundaries to equilibrate with annealing. This evidently has got more to do with their geometrical rearrangement rather than their relative energies. The continuous rearrangement of the boundaries seem to leave the volume fraction of the dominant cube componenet quite unaffected, as is clear from table 4.10. Since all the boundaries have been found to have similar energies particularly in the sample annealed at 50 hours in this investigation, it becomes immediately clear that none of the grains will have an advantage for preferential growth, thus keeping the volume fraction of the cube componenet more or less the same. The tendency of the energy ratio to move towards 1 can be explained as follows.

During deformation, lattice dislocations can easily run-in into high angle grain boundaries, thus creating extrinsic grain boundary discolations (EGBDs). Grain boundaries containing EGBDs posses higher energy and they can be transformed annealing to the low energy equilibrium state. As the material has been cold rolled to 95%, the grain boundaries even after annealing for small time periods are are in non equilibrium state. Table 5.1 to 5.5 shows γ_3/γ_1 and γ_2/γ_1 ratios greater than 1 and sometimes less than 1, this is due to the initial non equilibrium state of grain boundaries for lower annealing time. But with annealing for larger time periods they are attaining equilibrim state and therefore the distributions are tending to 1 with annealing.

The above conclusions are further expanded by the fact that the grain size distribution and fractal dimensions were similar in all samples. The only parameters that varied with annealing are the TDA and grain boundary energy values.

Chapter 6

Conclusions

---

1. The mean intercept length of the intercept length distributions are continuously increasing and this indicates an overall increase in the grain size on annealing. Analysis of standard deviation and the 95% confidence interval also suggest that the increase in grain size is statistically significant. However for the transformed spatial grain size distribution, 95% confidence interval cannot be determined because the standard deviation of the sampling distribution cannot be calculated.

2. From the normalised cumulative frequency curves of the intercept length distributions, it could be concluded that the grain size distribution of the 50 hours annealed is significantly different from the other grain size distributions. The complete overlapping of the cumulative frequency curves for the rest of the annealed samples implies that the differences of the microstructures are related to each other by a scale factor.

3. Matrix Method is a statistical way of obtaining spatial grain size distribution from linear intercept distribution, and therefore the transformed distribution is prone to statistical errors. On transformation some of the relative frequency values obtained are negative, (which were converted to zero) and this negative values should correspond to the relative frequency close to zero. This may also be due to the errors in intercept length measurements which were obtained manually from the micrographs.

4. A scatter in the cumulative frequency and normalised cumulative frequency curves of the transformed spatial grain size distribution was observed and hence it was difficult to compare them.

5. On transformation from PDA to TDA the spread of the distribution decreases and therefore the standard deviation values decreases and the peak height of the distribution increases significantly. The standard deviation values of true dihedral angles does not show much difference with annealing.

6. The two distributions of grain boundary energy ratios viz. γ_3/γ_1 (corresponding to the ratio of lowest to highest of the three TDA) and γ_2/γ_1 (corresponding to the ratio of second highest to highest of the three TDA) are tending towards 1 with annealing, and this suggests the equilibration of random grain boundarie.

7. As the grain boundaries are not much different from one another energy-wise, the grain boundary movement taking place during process is not dependent on individual grain boundary energies and as a result the continuous rearrangement of the boundaries is having no effect on the volume fraction of the dominating cube {100}<001> component and this suggest that none of the grain boundaries had an advantage of preferantial growth.

8. The calculated fractal dimension of all the annealed samples are close to 1, which suggests that the grain boundaries are not rugged.

9. Thus an important conclusion of this work is that, a correlation between texture and grain boundary energy distribution is possible. The grain size distribution and fractal dimension were similar in all the samples. The only parameters that varied with annealing are the TDA and grain boundary energy values.

The suggestions for future work:

1. Better results can be achieved from the technique to transform PDA to TDA, by accurate measurements of plane dihedral using an image analyser to cover a large area statistically.

2. An optimisation technique with the constraint that all the relative frequencies must be greater than or equal to zero for the determination of spatial grain

distribution is suggested. This is explained to reduce the scatter in the transformed frequencies.

3. Further investigations in this area of correlation of microstructural parameters with texture are suggested.

References

1. E.Schell and H.Wurst,Z.Metallkunde.,vol.23(1936),p:340.

2. N.A.Haroun,phd thesis,sheffield university,1967.

3. E.Schell,Z.Metallkunde.,vol.27(1935),p:199.

4. E.P.Papadakins,journal of applied physics.vol.35(1954),p:1586.

5. N.A.Haroun and M.S.Abdel-Azim,J.Inst.Met.vol.99(1971),p:319.

6. F.C.Hull and W.J.Houk.Trans.AIME,vol.197(1953),p:565.

7. N.A.Haroun,J Material science,vol.16(1981),p:2257.

8. Manabu Tanaka and Hiroshi Lizuka,Z.Metallkunde.,vol.82(1991),H.6,p:442.

9. Ingeborg,R.Gobel,Z.Metallkunde.,vol.82(1991),H.11,p:858.

10. B.B.Mandelbrot.et.al.,Nature,vol.19(1984),p:721.

11. Manabu Tanaka,Z.Metallkunde.,vol.84(1993),H.10,P:697.

12. A.Imre,Scripta Met.,vol.27(1992),p:1713.

13. Shu-Zu Lu,et.al.,Acta Metall.vol.42(1994),No.12,p:4035.

14. Su Hui ,et.al.,Scripta Met.,vol.25(1991),p:651.

15. Q.Y.Long,et,al.,Scripta Met.,vol.27(1992),p:1319.

16. K.K.Singh and S.sangal, Proceedings of the international conference on superplasticity in advanced materials,149,1997.

17. S. sangal, Metals, Materials and Processes, 4,1998.

18. B.P.Kashyap and K.Tangri.Acta Metall.,vol.43(1995),p:3971.

19. An Introduction To Textures in Metals, *by*, M. Hatherly and W.B.Hutchinson.

20. R.K.Ray, Unpublished Data.

A 131077

B 131077

Date Slip

This book is to be returned on the date last stamped.